Microbial loop of Proterozoic ocean analogue

Jaspreet S Saini[1,2], Christel Hassler[1], Rachel Cable[3], Marion Fourquez[7], Francesco Danza[4,5], Samuele Roman[4], Mauro Tonolla[4,5], Nicola Storelli[4,5], Stéphan Jacquet[7], Evgeny M. Zdobnov[2], Melissa B. Duhaime[3#]

[1]Department F.-A Forel for Environmental and Aquatic Sciences, Earth and Environmental Sciences, University of Geneva, Switzerland

[2]Department of Genetic Medicine and Development, University of Geneva, and Swiss Institute of Bioinformatics, Geneva, Switzerland

[3]Department of Ecology and Evolutionary Biology, University of Michigan, Ann Arbor, MI, United States

[4]Laboratory of Applied Microbiology (LMA), Department for environmental constructions and design (DACD), University of Applied Sciences and Arts of Southern Switzerland (SUPSI), Switzerland

[5]Department of Botany and Plant Biology, University of Geneva, Switzerland

[6]Université Savoie Mont-Blanc, INRAE, UMR CARRTEL, Thonon-les-Bains, France

[7]Aix Marseille Univ., Université de Toulon, CNRS, IRD, MIO UM 110, 13288, Marseille, France

Correspondent footnote

duhaimem@umich.edu

telephone 734-764-6219; fax 734-763-0544

Abstract

Meromictic Lake Cadagno, an ancient ocean analogue is known for its permanent stratification and persistent anoxygenic microbial bloom within the chemocline. Although the alpine lake has been extensively studied for at least 25 years, a comprehensive picture of the microbial food web relating phytoplankton, zooplankton, bacteria, and viruses is still missing. This study sought to better understand the abundances and productivity of microbes in the context of nutrient biogeochemical cycling across the stratified zones of Lake Cadagno. Photosynthetic pigments and chloroplast 16S rRNA gene phylogenies suggested the presence of eukaryotic microbial guilds in chemocline and oxic mixolimnion where oxygenic-primary production peaked. Anoxygenic phototroph, *Chromatium okenii,* was the most abundant bacteria along with the high abundances of *Lentimicrobium* whose members are known to perform fermentation. Secondary production peaked in the chemocline suggesting that primary producers rely on heterotrophs for nutrients remineralization. Virus-to-microbe ratios (VMR) peaked in the zone of phytoplankton and were minimum at the peak *Chromatium okenii* hinting viruses modulating oxygenic and anoxygenic photo-and-chemosynthesis.

Significance

This study provides a window to the past on how microbial guilds of the chemocline may have functioned towards the production and recycling of organic matter in vertical water-columns of sulfur- and ammonia-containing ancient oceans, which slowly evolved to modern oxygenated systems. New observations of this work suggest that eukaryotic algae were persistent in the low oxygen upper-chemocline where they were found to be associated with purple sulfur and green sulfur bacteria in the lower half of the chemocline. This study provides the first insights into Lake Cadagno viral ecology. High viral abundances suggest viruses were essential components of the chemocline where they may cause the release and recycling of organic matter. The framework developed in this study through the integration of a multitude of geochemical and biological data lays the foundation for future studies to further resolve the microbial loop in this early anoxic ocean analogue.

Introduction

Roughly 2.3 billion years ago the oceans were filled with sulfur [1]. Anoxygenic photosynthesis was a dominant mode of microbial primary production [2–4]. Following the great oxidation event (~2 Gyr), anoxygenic photosynthesis continued to sustain microbial life in euxinic environments below oxygenated surface waters [1,3,5]. Habitats in which anoxygenic photosynthesis significantly contributes to primary production continue to persist, such as in anoxic zones of permanently stratified sulfur-rich meromictic lakes like Lake Cadagno [6] where hydrogen sulfide is used as an electron donor [7]. These permanently stratified lakes are resistant to seasonal mixing events that would otherwise redistribute oxygen throughout the water column [8]. In these systems, biogeochemical processes provide a link between the contrasting dominant modes of primary production, thereby directly connecting the food webs of the oxygenated and anoxic habitats.

The microbial community composition of meromictic Lake Cadagno typifies the reconstructed signatures of life in the Proterozoic ocean [9,10]. Purple and green sulfur bacteria (PSB and GSB, respectively) are amongst the hallmark bloom-forming microbes that are frequently observed in the chemocline of Lake Cadagno [11,12]. Within the chemocline, carbon, nitrogen, sulfur, and iron cycling are integrated through metabolic activities of the anoxygenic photosynthetic purple sulfur and green sulfur bacteria [13–16]. Two purple sulfur bacteria, *Thiodictyon syntrophicum* and *Chromatium okenii*, have been identified as the greatest contributors to primary production in Lake Cadagno [12,14,17]. However, measurements of primary production to date have been limited to the chemocline [12,18] and measurements of secondary production do not exist. Phytoplankton (including modern eukaryotes and cyanobacteria) evolved in Proterozoic oceans [19,20], and their recurrence with anoxygenic phototrophic sulfur bacteria are known in the ancient aquatic systems [21]. Phytoplankton abundance and productivity were expected to be prevalent in the oxic zone because phytoplankton produces organic matter via oxygenic photosynthesis. In order to better understand microbial loop linkages across the stratified mixolimnion-chemocline transition in Lake Cadagno, paired measurements of productivity, microbial community composition and diversity are essential next steps.

Lake Cadagno studies to date have focused on the phytoplankton and prokaryotic members of the microbial community and have yet to include viruses. Viruses are known to impact both phytoplankton and heterotrophic microbial populations through lysis and lysogeny and may hold a central position in the marine food webs and biogeochemical cycling [22–25]. Through the lysis of

their microbial hosts, viruses play a role in the conversion of particulate organic carbon to dissolved organic carbon, which is predicted to be capable of sustaining the microbial loop [26,27]. Viruses have been identified in meromictic lakes [28–30], but their abundances across the vertical water column of Lake Cadagno are unknown.

To better understand the role the microbial loop plays in sustaining the food web across the stratified layers of Lake Cadagno, microbial community members (phytoplankton, prokaryotes, and viruses) were studied in the context of biogeochemical and production (primary and secondary) measurements across the oxic-anoxic transitions of the meromictic Lake Cadagno [9,13]. We hypothesized the mixolimnion to have low primary production as compared to the chemocline because chemocline is inhabited by a persistent microbial bloom of primary producing phototrophic sulfur bacteria [12]. We also expected high secondary production and viral abundance to be an indicator of effective organic matter recycling within the Lake Cadagno water column because photoautotrophs, both phototrophic sulfur bacteria and phytoplankton, rely on heterotrophs and viruses for the remineralization of organic matter and nutrient cycling [31,32]. Through a combination of physical, chemical and biological analyses, this work provides new evidence on how transitions between permanently stratified lake habitats and assemblages may sustain microbial food webs and informs our understanding of the aquatic ecosystems of early Earth.

Results

Position of Mixolimnion, Chemocline, and Monimolimnion

Transitions between the major stratified layers sampled from Lake Cadagno were visually apparent by the colour of pigmented biomass captured on the 0.22 µm filters (Fig. 1A). From the surface to 12.5 m depth, the oxygen levels fell from a maximum of 9.24 mg/L to 2.79 mg/L (light green, day 2; Fig. 1B). As hypoxia is defined as 2 mg O_2/L [33], 12.5 m marks the boundary of the oxic mixolimnion zone and the upper chemocline (top light purple; Fig. 1). The chemocline was 13.5-15.5 m, as determined based on near-zero oxygen and light levels (day 2), peaked turbidity, a sharp decrease in temperature, and a simultaneous rise in conductivity (dark purple; Fig. 1, B-D). At 14.5 m, oxygen levels were below detection and <1% of surface light penetrated (day 2; Fig. 1B, D). Within the chemocline, the deep chlorophyll maximum (DCM) and peak turbidity shifted

overnight between days 1 and 2, but in both cases, the peak turbidity was observed 0.5-1.5 m below the DCM (day 2; Fig. 1B, D). Peak phycocyanin concentrations (26.53 µg/L) and basal fluorescence (Fb= 66.0) were observed at the DCM (day 2, 13.5-14 m) and above a secondary chlorophyll peak at 15 m (Fig. 1D, Fig. S1E). The monimolimnion was defined as the zone between 15.5 m and the benthos. The peak in particulate sulfur (0.74 ppm), H_2S (2.84 mg/L) and ammonia (262.4 µg/L) concentrations were observed in the monimolimnion, as well as a decline in turbidity and photosynthetic pigments (Fig. 1B, E, H).

Microbial production at the oxic/anoxic interface

Between 7-11 m in the lower mixolimnion, there was a slight rise (up to 13.12 µg/l on day 1 and 11.80 µg/l on day 2) in Chl *a* (Fig. 1D). The Chl *a* peak in the mixolimnion at 9 m corresponded with a peak in net primary production (NPP; 3210 ng C l^{-1} h^{-1}; Fig. 1D, F). The NPP peak declined in the lower mixolimnion (11 m) and upper chemocline (13 m). Though NPP was not measured below 13 m, basal and maximum fluorescence measured through the chemocline gave an indication of photosynthetic activity and efficiency (Fig. S1E). In the oxic-anoxic boundary, a maximum Fv/Fm (an indicator of photosynthetic efficiency) of 0.49 was observed between 13-13.5 m and declined to 0.36 at 15 m (Fig. 1F). Overlapping with this oxygenic photosynthesis, the highest rates of secondary productivity (SP) were observed through the chemocline (Fig.1F). SP was significantly positively associated with some indicators of both photosynthetic microbes (Pearson: Chl *a*: R=0.96, p-value=1.7e-5; phycocyanin: R=0.80, p-value=0.005) and total biomass (Pearson: turbidity: R=0.78, p-value=0.007; total cell counts: R=0.65, p-value=0.04) (Fig. S2). In the chemocline, SP and indicators of NPP (phycocyanin, Chl a) were significantly negatively correlated with oxygen and light (Pearson: R=-0.7 to -0.9, p-values = 0.0002 to 0.01; Fig.S2). The peak of DOC (14 m) were followed by peaks of POC, PON (15 m; Fig. 1G-H). In the monimolimnion below the chemocline, some organic and inorganic compounds continued to rise (POS, H_2S, NH_4^+), while PON and POC dropped (Fig. 1).

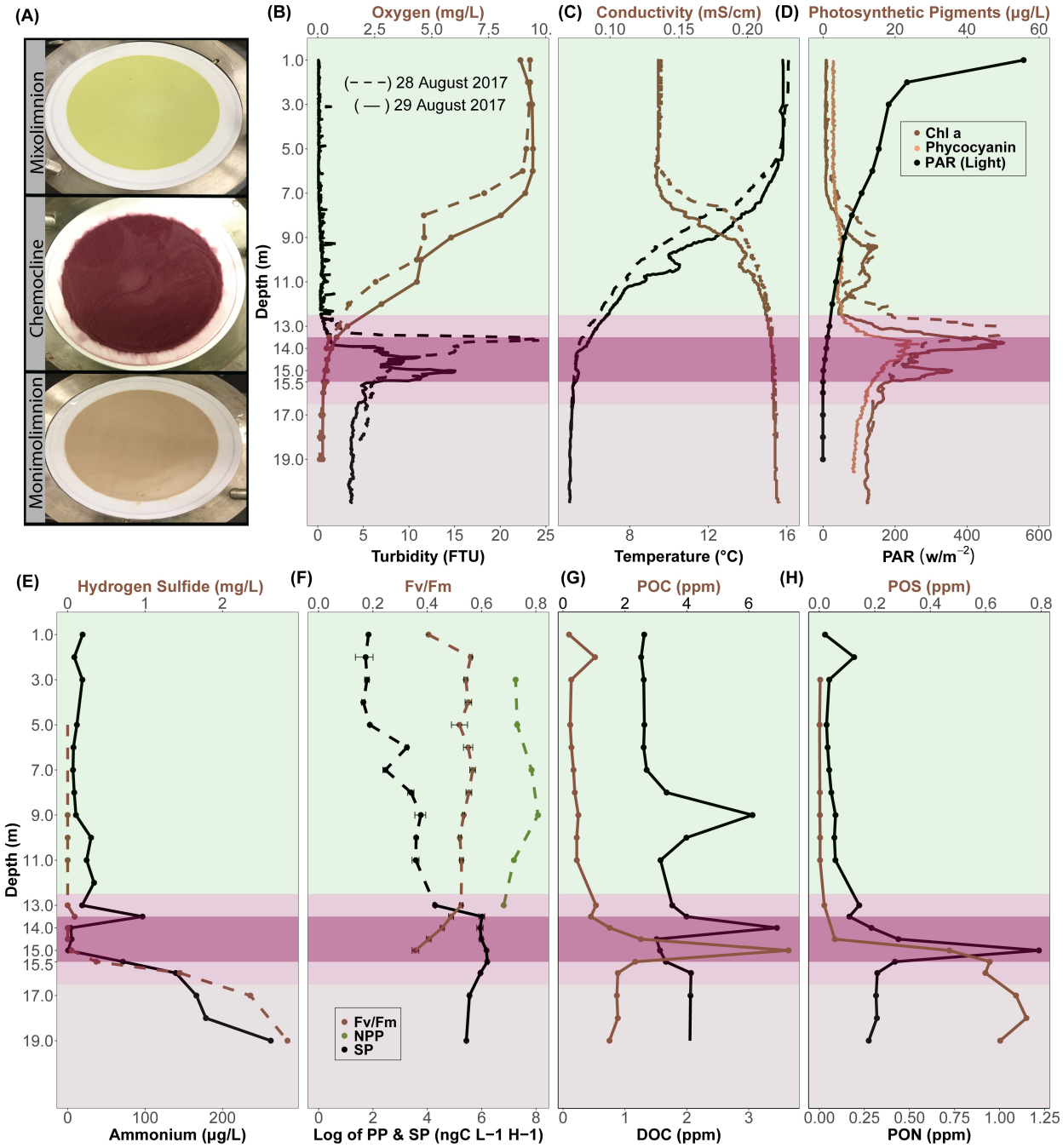
(A)
Mixolimnion
Chemocline
Monimolimnion
(B)
Oxygen (mg/L)
(- - -) 28 August 2017
(—) 29 August 2017
Depth (m)
Turbidity (FTU)
(C)
Conductivity (mS/cm)
Temperature (°C)
(D)
Photosynthetic Pigments (µg/L)
Chl a
Phycocyanin
PAR (Light)
PAR (w/m-2)
(E)
Hydrogen Sulfide (mg/L)
Ammonium (µg/L)
(F)
Fv/Fm
Fv/Fm
NPP
SP
Log of PP & SP (ngC L−1 H−1)
(G)
POC (ppm)
DOC (ppm)
(H)
POS (ppm)
PON (ppm)

146

Figure 1. Depth profiles of biogeochemical parameters of Lake Cadagno. (A) Photographs of biomass collected on 0.22 µm (142 mm diameter) filters from Lake Cadagno mixolimnion, chemocline, and monimolimnion strata. The depth profiles of (B) oxygen and turbidity, (C) conductivity and temperature, (D) Chl *a*, phycocyanin, and photosynthetically active radiation (PAR) (E) hydrogen sulfide and ammonium, (F) net primary production (NPP) and secondary production (SP), (G) particulate organic carbon (POC) and dissolved organic carbon (DOC), (F) particulate organic sulfur (POS) and particulate organic nitrogen (PON). In B-H, the mixolimnion, chemocline transition zone, chemocline, and monimolimnion layers are indicated by light green, lilac, purple and light brown backgrounds, respectively. Dashed and solid lines represent 28th and 29th August 2017, respectively.

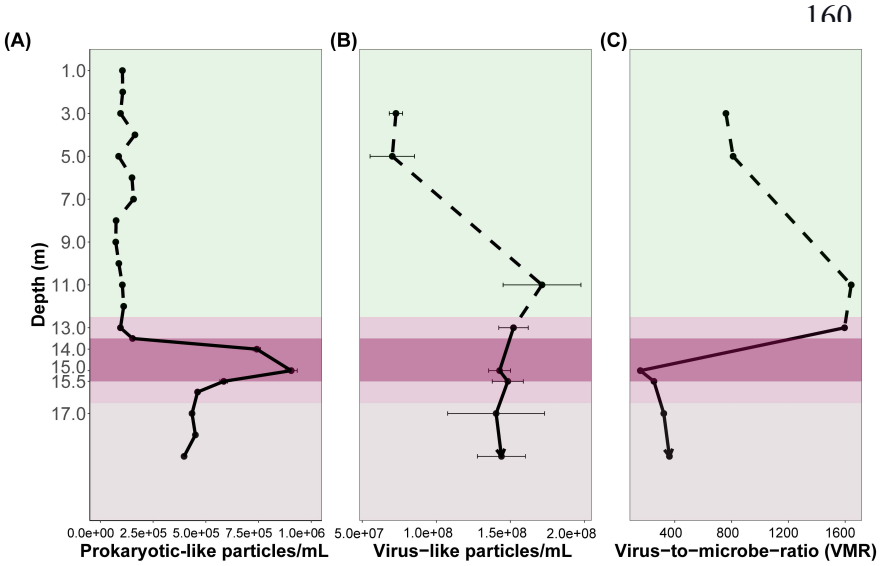

Figure 2. The abundance of (A) prokaryote-like particles (PLP) and (B) virus-like particles (VLP) from flow cytometry analyses and (C) virus-to-microbe ratio, as VLP/PLP.

Prokaryote- and Virus-like-particle abundances and trends

The concentration of prokaryotic-like particles (PLPs; prokaryotic cell counts inferred from flow cytometry data) was highest in the chemocline (905,000 cells/ml ± 28,583 at peak, 496,000 ± 17,295 avg cells/ml), lower in the monimolimnion (435,833 ± 10,243 avg cells/ml), and was lowest in the mixolimnion (109,556 ± 3,496 avg cells/ml). In contrast, virus-like particles (VLPs; viral counts inferred from flow cytometry data) were highest at the bottom of the mixolimnion and were relatively invariable through the rest of the water column (Fig. 2B). As a result, the virus to microbe

177 ratio (VMR) peaked with viruses at the bottom of the mixolimnion but decreased drastically when
178 prokaryotic-like particles rose in the chemocline (Fig. 2).
179 Significant positive correlations were observed between PLP concentrations and other
180 indicators of biomass: turbidity (R=0.95; p-value=0.00003), Chl *a* (R=0.76; p-value=0.01), POC
181 R=0.92; p-value=0.0001), PON (R=0.93; p-value=0.0001), and POS R=0.76; p-value=0.010) (Fig.
182 S3). Of those, only the VLP concentrations were correlated with Chl *a* (R=0.77; p-value=0.02,
183 (Fig. S4). Significant negative correlations were observed between VLPs and oxygen (R=-0.82, p-
184 value=0.01) and light R=-0.90, 0.002). Significant positive correlations were observed between
185 VLP and depth (R=0.78, p-value=0.02), conductivity (R=0.92, p-value=0.001), and SP (R=0.70;
186 p-value=0.05) (Fig. S4).
187
188 **Bacterial community composition through the mixolimnion, chemocline, and**
189 **monimolimnion**
190 Absolute abundances of Bacteria-classified cells (16S rRNA gene read abundances scaled by total
191 FCM PLP counts at each depth) were at a minimum in the oxic mixolimnion (0-12.5 m; Fig. 3, SI
192 Table 1). In this zone, the community primarily consisted of Actinobacteria, Bacteroidetes,
193 Proteobacteria, and Cyanobacteria phyla (Fig. 3A, Fig. S5). The relative abundance of
194 Cyanobacteria peaked in the mixolimnion to chemocline transition zone at 13 m, where the phylum
195 comprised 24.53% of the total community (23,387 cells/ml; Fig. S5).
196 In the chemocline, at 15 m (day 2) the absolute abundance of Bacteria-classified cells
197 peaked (Fig. 3A), which corresponded with peak turbidity, POC and PON (Fig. 1). The major
198 phyla represented at this depth were Proteobacteria (48.42% of total Bacteria, 438,272 cells/ml)
199 and Bacteroidetes (25.35% of total Bacteria, 229,448 cells/ml). The genera that dominated these
200 phyla at 15 m were purple sulfur bacteria *Chromatium* (35.18% of total Bacteria, 318,381 cells/ml;
201 Proteobacteria). *Chromatium* was significantly positively correlated with turbidity (R=0.93; p-
202 value=7.3e-5) and total cell counts (R=0.99; p-value=8.2e-09) (Fig.6 A-B). An unclassified
203 *Lentimicrobiaceae* OTU, the second most abundant OTU, was significantly positively correlated
204 with secondary production (*R*=0.8*;* p-value=0.005), turbidity (R=0.91, p-value=0.0002), PLPs
205 (R=0.85, p-value=0.001), PON (R=0.71, p-value=0.02), POS (R=0.92; p-value=5e−04), yet,
206 negatively correlated with light (*R*=-0.78*,* p-value=0.007, Fig.S6H) and oxygen concentration

207 (*R*=-0.87*;* p-value=0.001; Fig. S6C-I). Though Firmicutes was not a dominant phylum itself, an
208 unclassified genus of *Erysipelotrichaceae* (3.90%, 35,360 cells/ml; Firmicutes) was also among
209 the dominant genera at 15 m (SI Table 1). In addition to *Chromatium* (purple sulfur bacteria,
210 PSBs), other PSBs found to be involved in primary production in the Lake Cadagno chemocline
211 [12,15], *Thiodictyon* and *Lamprocystis* were observed at low abundances at 15 m (7.16e-04%, 649
212 cells/ml, and 4.09e-03%, 3,707 cells/ml, respectively; SI Table 1). Apart from PSBs, green sulfur
213 bacteria *Chlorobium* (2.29%, 20,808 cells/ml) was the fifth most abundant genera of chemocline.
214 Also in chemocline at 15 m, previously observed sulfur-reducing genera [34,35], *Desulfocapsa*,
215 *Desulfobulbus*, were also observed at low abundances (5,098 cells/ml, 0.005% and 1,854 cells/ml,
216 0.002%, respectively; SI Table 1).
217 In monimolimnion (17-19 m), the relative community composition reflected that of the
218 chemocline, while OTU absolute abundances decreased (Fig. 3A). The same genera reported
219 above to dominate the chemocline at 15 m were found to dominate the monimolimnion depths. In
220 addition to bacteria, this study also found archaeal OTUs (genus methanoregula, Woesearchaeia)
221 in monimolimnion but was not considered further because of a significantly low abundance
222 overall (<100 OTUs, SI Table 3).

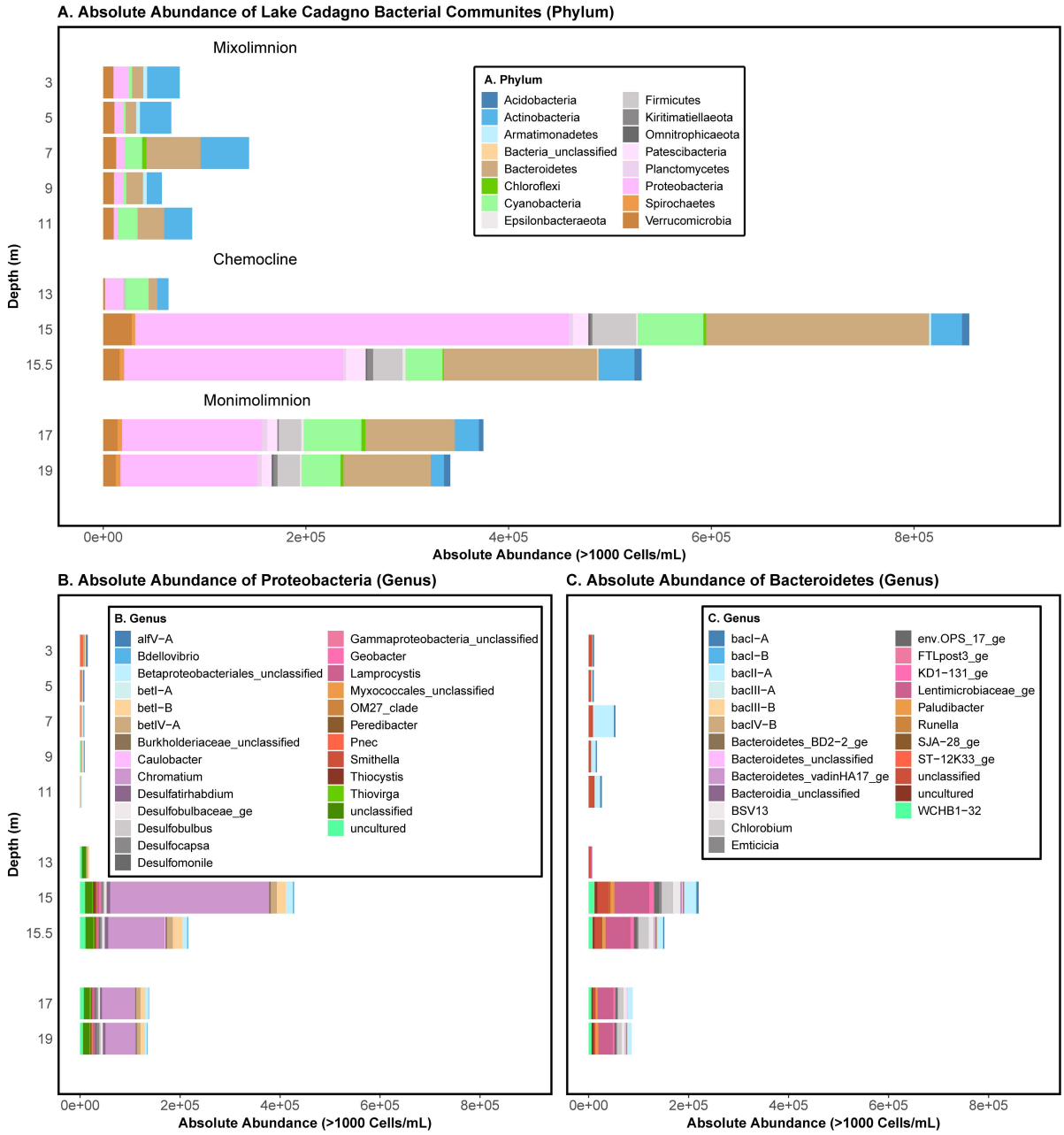

Figure 3: At the sampled depths in Lake Cadagno, absolute abundances (cells/ml) of (A) bacteria phyla, (B) genera in the Proteobacteria phylum, (C) genera in the Bacteroidetes phylum. To the right of each panel, the mixolimnion, chemocline transition zone, chemocline, and monimolimnion layers are indicated by light green, lilac, purple and light brown backgrounds, respectively and correspond with the depths reported on the y-axis to the left.

231 **Oxygenic phototrophs in the mixolimnion, chemocline, and monimolimnion**

232 At the phylum level, Cyanobacteria was among the top phyla consistently observed at each
233 depth in the water column, but at no depth did it dominate (Fig. 3A). At all depths,
234 *Oxyphotobacteria* and chloroplast-classified OTUs dominated the Cyanobacteria phyla,
235 representing 94-100% of the total Cyanobacteria-classified OTUs. Three other low abundance
236 genera classified as belonging to the Cyanobacteria phylum included *Cyanobium* (throughout the
237 water column), *Pseudanabaena* (predominantly 15 m and below, Fig. 4A-B), and
238 *Gastranaerophilales* (predominantly 15 m and below, Fig. 4A-B). We sought to derive more
239 information about the origin of these putative chloroplast OTUs. The phylogeny of all
240 Cyanobacteria-classified OTUs and their two nearest neighbours in SILVA [36] indicated that the
241 chloroplast and *Oxyphotobacteria* OTUs clustered in clades with chloroplast 16S rRNA genes of
242 cultured eukaryotic algae (Fig.4B): Chlorophyta (Otu00008, Otu000342, Otu00006, Otu00323),
243 Ochrophyta (Otu00033), Streptophyta (Otu00208), Haptophyta (Otu00143), and uncultured-
244 chloroplasts (Otu00042, Otu00051, Otu00052, Otu00055).

245 In the lower mixolimnion between 7-11 m, where high oxygen, *chl a*, and NPP persisted
246 and peak Fv/Fm was observed (Fig. 1D, F), Otu00008, which belonged to the same clade as the
247 chloroplast genome of *Ankyra judayi*, a cultured Chlorophyta, dominated the subset of
248 Cyanobacteria-classified OTUs and ranged in absolute abundance from 1810 to 17,340 cells/ml
249 (Fig. 4B, D). At 11 m, the next most abundant OTUs were Otu00042 and Otu00055, which
250 belonged to a clade of uncultured chloroplasts and were observed at 4316 and 6341cells/ml,
251 respectively.

252 At the chemocline DCM between 13-14 m, flow cytometry-based counts phycobilin-
253 containing cells (309,333 cells/ml; Fig.4C), phycocyanin pigments (26 µg/l day 2, Fig1D), and
254 Chl *a* pigments (45 µg/l day 2) rose sharply (day 2; Fig. 1D). At this depth, Cyanobacteria-
255 classified OTUs represented 24.53% of total reads and 23,387 cells/ml. At the secondary peak of
256 chlorophyll (15 m), Cyanobacteria-classified OTUs represented 7.28% of total reads and 65,947
257 cells/ml (SI Table 2). The most abundant chloroplast OTU throughout the chemocline, Otu00006,
258 belonged to a clade with the chloroplasts of cultured Chlorophyta species, *Parachlorella kessleri*
259 and *Closteriopsis acicularis* (Fig. 4D). The next most dominant chloroplast-like OTUs, Otu00033
260 and Otu00052, clustered with cultured Ochrophyta chloroplasts and uncultured chloroplasts,
261 respectively (Fig. 4D). In the monimolimnion, Otu00006 and Otu00033 dominated the

Cyanobacteria-classified OTUs (Fig. 4D), which belong to Chlorophyta and Ochrophyta chloroplast clades, respectively.

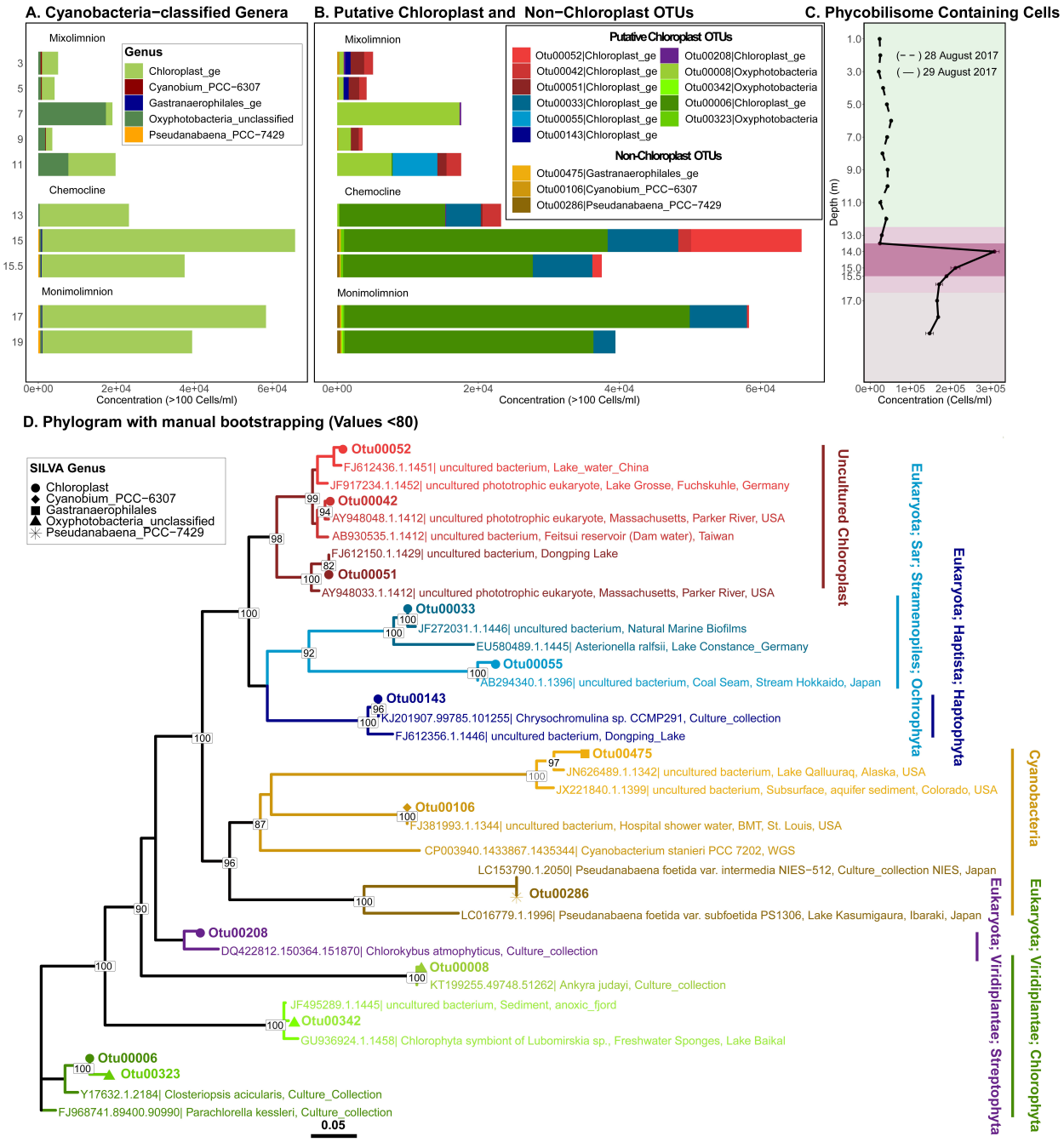

266 **Figure. 4:** Abundance of phototrophs based on flow-cytometry counts and 16S rRNA sequencing.
267 Mixolimnion samples (0-11 m) were collected on day 1, chemocline and monimolimnion (12-19
268 m) samples were collected on day 2. Abundances in panels B-C are acquired by scaling OTU read
269 counts by FCM cell counts. (A) Concentrations (cells/ml) of OTUs classified as belonging to the
270 Cyanobacteria phylum. (B) Concentrations (cells/ml) of OTUs are classified as putative
271 chloroplasts and non-chloroplast at the genus level assigned within phylum cyanobacteria. (C)
272 Depth profile of phycobilins-containing cell counts based on flow cytometry with a 640 nm laser.
273 The mixolimnion, chemocline transition zone, chemocline, and monimolimnion layers are
274 indicated by light green, lilac, purple and light brown backgrounds, respectively. (D) Phylogenetic
275 tree of the representative 16S rRNA gene amplicon sequences of putative chloroplast and non-
276 chloroplast OTUs in panel B along with their two nearest neighbour sequences from the SILVA
277 database. Clades are colour-coded consistent with the colouring of bar plots in prior panels.
278

279 **Prokaryotic genotypic and phenotypic diversity trends**

280 Bacterial genotypic diversity and PLP phenotypic diversity (based on individual cell features
281 distinguished by the cytometer; [37] both dropped at 7 m and rose in lower mixolimnion where
282 oxygenic primary production peaked (Fig. 5A-B, Fig. 1F). Overall, genotypic alpha diversity
283 (Shannon) trends were near-uniform, except at the peak of turbidity (15 m) where PLP phenotypic
284 alpha diversity peaked and moderate genotypic alpha diversity was observed (Fig. 5A-B). Below
285 chemocline, consistently high genotypic and phenotypic alpha diversity was observed in the anoxic
286 monimolimnion. In the Principal Coordinate Analysis (PCoA) ordinations of genotypic and
287 phenotypic diversity, the first two PCs of bacterial community dissimilarity (Bray Curtis)
288 accounted for 77% and 46.2% of all observed variation in genotypic and phenotypic beta diversity,
289 respectively (Fig. 5 C-D). Oxic (mixolimnion, green) and anoxic (monimolimnion, light brown)
290 samples separated along with the first principle component (PC1) (Fig. 5 C-D), which explained
291 66.6% and 29.8% and of the total variation in sample dissimilarity, for the genotypic and
292 phenotypic beta diversity, respectively. In the phenotypic diversity ordination (Fig. 5), the
293 mixolimnion samples separated along PC2 (alone explaining 16.4% total variation) by whether
294 they originated from the high-oxygen (1-7 m, light green) or the mid-oxygen (8-11 m, dark green)

295 zones (Fig. 5 C-D). As with bacterial phenotypic alpha diversity, oxygen and light were negatively
296 correlated with bacterial phenotypic and genotypic beta diversity (Fig. S7).
297

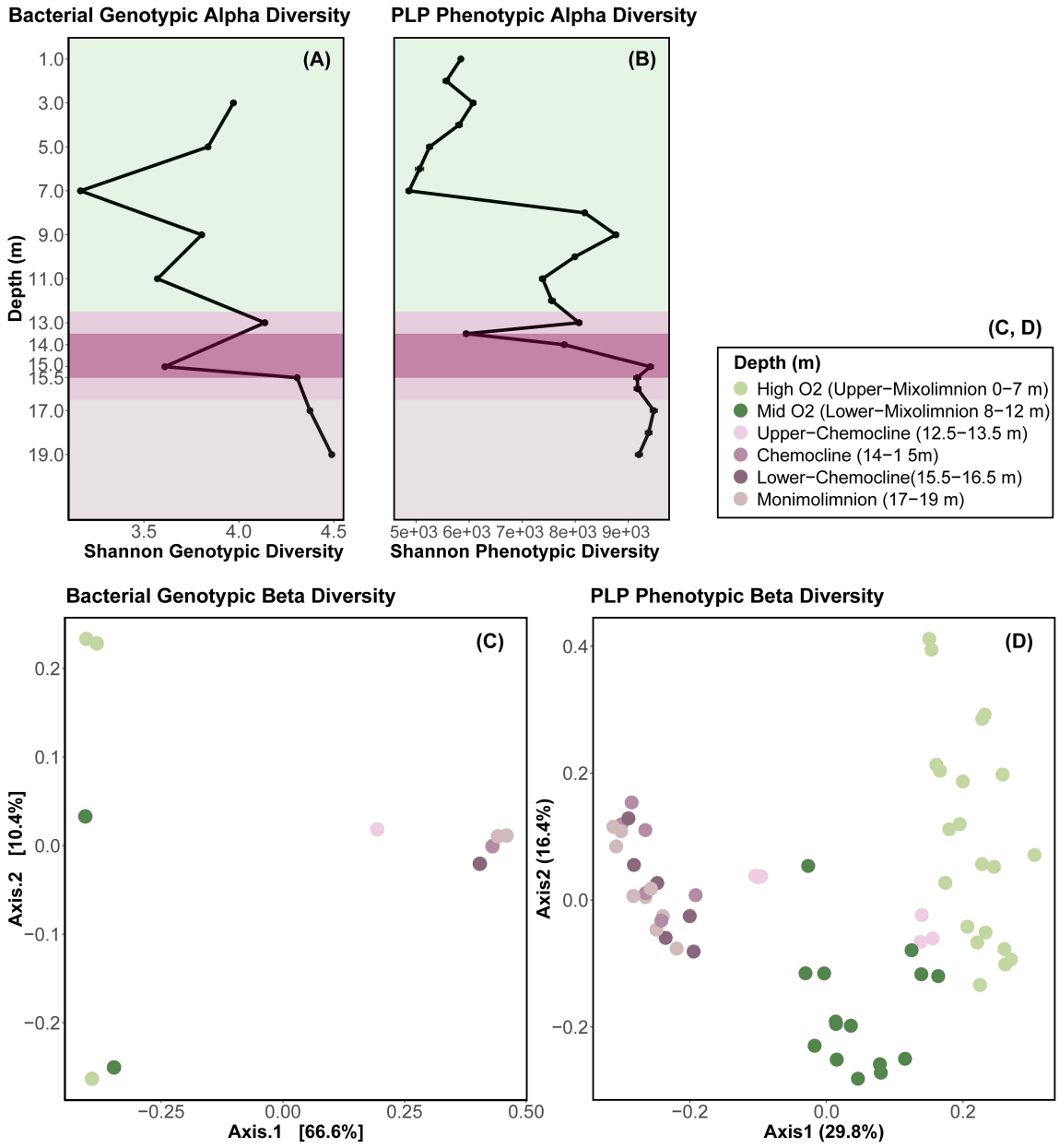

298

Figure. 5: Trends in microbial community genotypic (16S rRNA gene amplicon sequencing) and phenotypic (flow-cytometry) diversity in Lake Cadagno. (A) Shannon diversity index depicting genotypic diversity of bacterial communities including chloroplasts OTUs (16S rRNA gene amplicon sequencing). The mixolimnion, chemocline transition zone, chemocline, and monimolimnion layers are indicated by light green, lilac, purple and light brown backgrounds, respectively. (B) Phenotypic alpha-diversity (Shannon) of microbial communities with depth in Lake Cadagno. Mixolimnion samples (0-11 m) were collected on day 1, chemocline and monimolimnion (12-19 m) samples were collected on day 2. Data are represented colour-coded according to sampling depths. (C) PCoA of beta diversity of bacterial communities (16S rRNA gene sequencing including chloroplast-like OTUs) based on the Bray-Curtis dissimilarity metric. (D) PCoA ordination representing sample distances inferred from phenotypic beta diversity measures (Bray Curtis distance) of microbial communities based on PLP flow cytometry data.

Discussion

In this study, the investigation of microbial and biogeochemical dynamics through Lake Cadagno's water column improves our understanding of the connectivity of spatially segregated food webs in the Proterozoic ocean model [3].

Eukaryotic algae associated with oxygenic phototrophy in the mixolimnion

With the transition of OMZ chemistry at 800-700 Ma, the reduced levels of sulfur and ammonia likely facilitated the eukaryotic evolution as proposed in the Proterozoic ocean model [3]. The low sulfur and ammonia along with the relatively low number of small (<40 µm) prokaryotic-like particles, in combination with the high number of chloroplast 16S rRNA gene reads in the zone of oxygenic photosynthesis support the eukaryotic trend in mixolimnion of this study (Fig. 6A). The chloroplasts signals further suggest a high abundance of eukaryotic algae throughout the mixolimnion, specifically the freshwater chlorophyte, *Ankyra judayi* (Chlorophyta; OTU00008), which has not yet been described in Lake Cadagno (Fig. 6B). *Ankyra judayi* has been observed to outcompete other phytoplankton and grow to high densities in a high-alpine Andean lake, which was attributed to its ability to endure high UV radiation [38] and may explain its presence in the sun-lit mixolimnion of high-alpine Lake Cadagno. Our findings are consistent with prior microscopy-based studies that have reported that the majority of the algal biomass was attributed to eukaryotic

algae, such as *Echinocoleum* and *Cryptomonas* (Chlorophyta) and diatoms [18]. Overall, these observations match the predictions about the evolution of eukaryotes in low sulfur and ammonia and further suggests that the mixolimnion represents the conditions of modern aquatic systems.

Coexistence of oxygenic and anoxygenic primary producers in chemocline

The processes of the major microbial oxygenic and anoxygenic guilds have been reported to contribute almost equally to organic matter production in the Lake Cadagno chemocline [18], as they may have in ancient ocean chemoclines. Oxygenic (Chlorophytes, Diatoms, Cyanobacteria) and anoxygenic phototrophs (PSB and GSB) coexisted in the chemocline of this study (Fig. 6 C-E). Previous studies also reported cyanobacterial bloom (28 August, 12 September 2017) at the oxic-anoxic transition directly above the phototrophic sulfur bacteria [39,40], however, cyanobacteria (*Cyanobium*, *Gastranaerophilales, Pseudanabaena*) were rare in this report. Furthermore, the shift of oxygenic to anoxygenic photosynthesis is coincident with a decreasing efficiency of oxygenic photosynthetic microbes (F_v/F_m), increasing concentrations of hydrogen sulfide, and a shift in bacterial abundance and beta-diversity (Fig. 6F). When considering oxygenic and anoxygenic photosynthesis, nitrogen cycle was proposed to provide inorganic nitrogen essential for photoautotrophs in ancient oceans [3]. The peak in PON, and the rise in biologically accessible N (ammonia) at the peak turbidity supports the N-fixation trend in Lake Cadagno chemocline. The N-fixation mechanism likely carried out by the major carbon assimilators; PSB (*Chromatium, Thiodictyon*) and GSB (*Chlorobium*) of chemocline, which exhibited genes involved (*nif*) in nitrogen fixation [10,13,41,42]. Their diazotrophic metabolism may have provided PSB and GSB an ecological advantage for organic matter production (POC, PON, POS) in the chemocline of Lake Cadagno (Fig. 6G), and that explains PSB and GSB persistence in the 1.6Gyr old ocean basin of permanently stratified paleoproterozoic sea [43].

Apart from oxygenic and anoxygenic primary production, aerobic respiration also proposed to be contributed to the organic matter production in ancient ocean chemocline [3]. However, information on microbes associated with such activity was missing from the model. *Chromatium,* the most abundant microbe of chemocline in this study, was previously reported to carry out aerobic sulfide oxidation which contributed to 40% of total dark carbon fixation [44] (Fig. 6L). This aerobic respiration by *Chromatium okenii* was coupled with *in-situ* production of oxygen by photosynthetic algae [44]. Such *in situ* oxygenic production in Lake Cadagno was also associated

with methane oxidation by methanotrophs and iron oxidation likely by *Chlorobium* and *Rhodobacter*, where iron oxidation solely accounted for 10% of total primary production of chemocline [45,46] (Fig. 6H). The coexisting oxygenic phototrophs (Chlorophytes, Diatoms, Cyanobacteria) observed in this report might be contributing to the *in situ* oxygen production in the chemocline of Lake Cadagno. Therefore, future work is needed to understand the metabolisms of Chlorophytes, diatoms, cyanobacteria present in the oxic-anoxic interface of Lake Cadagno. Altogether, our observations fit the prediction of the Proterozoic ocean model which proposed a mixed community of oxygenic and anoxygenic primary producers typified by decreasing oxygen and increasing sulfide concentrations [3].

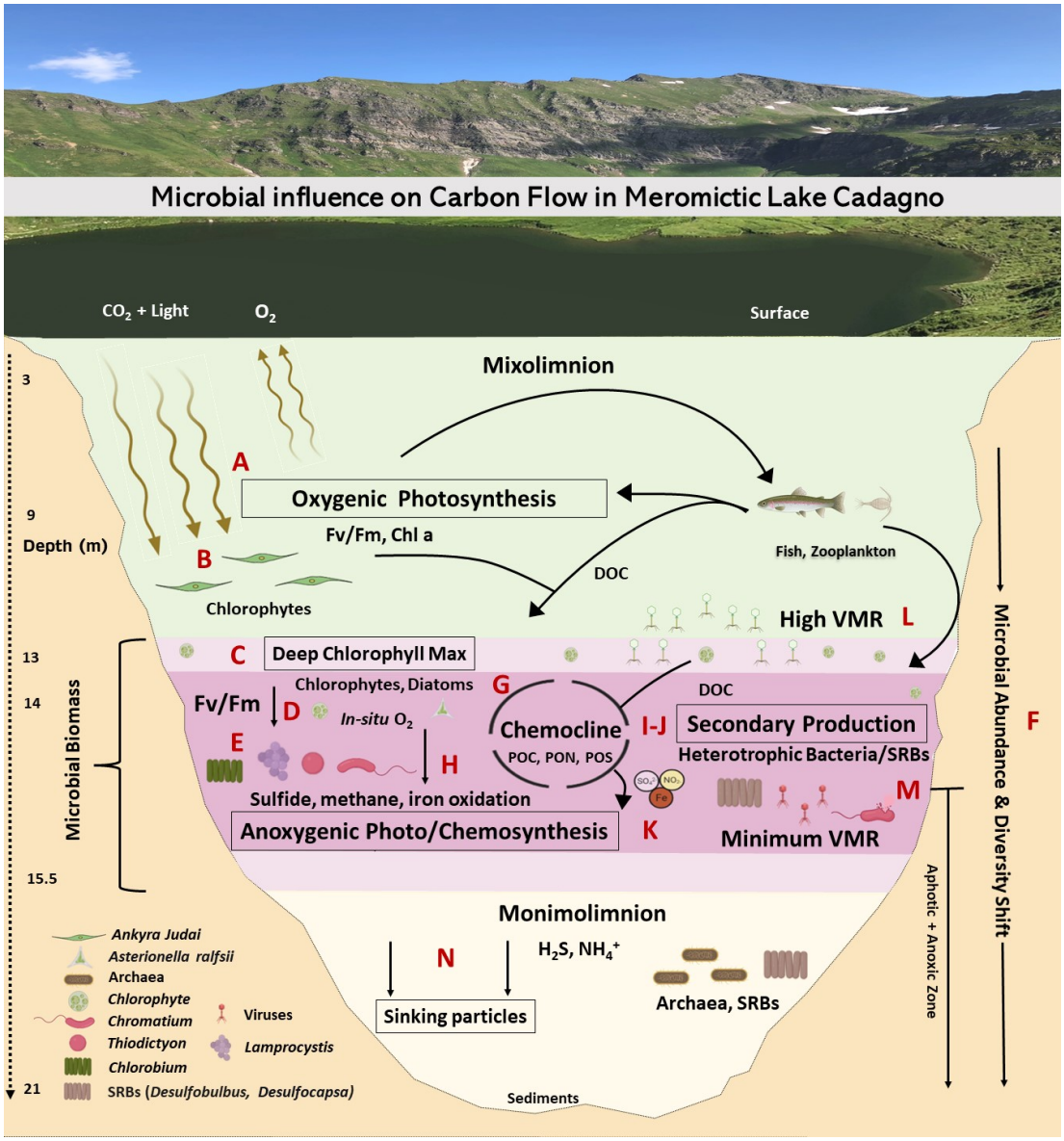

Figure. 6: Microbial loop of meromictic Lake Cadagno.

372

373 **Nutrient remineralization through secondary production contributes to chemocline biomass**

374 The purple sulfur bacteria (PSB), such as *Chromatium, Lamprocystis and Thiodictyon*, and
375 green sulfur bacteria (GSB), such as *Chlorobium,* that dominated the Lake Cadagno chemocline,
376 are known to be largely responsible for anoxygenic photo-chemosynthesis in this stratum (Fig. 6E)
377 [12,47], In this first report of secondary production in Lake Cadagno, we found that rates were the
378 highest in the chemocline, like primary production [12,14,17,18], exceeding rates in the mixolimnion
379 and monimolimnion by 42.4- and 1.9-fold, respectively (Fig. 6I).
380 *Lentimicrobium,* the second most abundant genus in this report, has strongly implicated
381 fermentation characteristics under limited light and oxygen in previous studies [48]. Heterotrophic
382 sulfur-reducing bacteria (SRBs, Fig. 6J), such as the observed *Desulfocapsa* and *Desulfobulbus,*
383 are known to associate with phototrophic PSB (e.g., *Chromatium okenii*, *Lamprocystis purpurea*)
384 and were both also observed in the chemocline [34,35]. The presence of such heterotrophic microbes
385 likely be decomposing particulate organic matter (POC, PON, POS), and supplying inorganic
386 nutrients (iron, sulfate, and nitrogen) necessary to carry out primary production of chemocline
387 (Fig. 6K). Thus contributing to maintaining the biomass of oxygenic and anoxygenic
388 photoautotrophs observed in the chemocline. Lastly, these autotrophic and heterophic relations
389 along with the secondary productivity rates provide the evidence on microbes involved in recycling
390 of organic matter proposed in the Proterozoic ocean model [3].
391

392 **Potential for viral modulation of phytoplankton and PSB activity**

393 Viruses were proposed to have a substantial impact on ancient cyanobacterial mats by
394 encoding the nblA gene responsible for degrading phycobilisomes, a pigment central to
395 photosynthesis [49]. They can also act as top-down controls on host populations and reprogram host
396 metabolism during infection [24,25,50]. VMR peaked in the lower mixolimnion and mixolimnion-
397 chemocline transition where high VLP and chlorophyll concentrations and high photosynthetic
398 activity were observed together with low bacterial abundances. Such coexistence between high
399 viral loads and highly active phytoplankton populations could be explained by ongoing lytic viral
400 infections of phytoplankton near the DCM (Fig. 6L). Such a scenario was observed in the
401 phytoplankton *Ostreococcus* virus-host system, where host densities were maintained concurrently

402 with continual lysis due to phase switching between resistant and susceptible host, a strategy
403 supported by mathematical modeling [51]. If this scenario is occurring, the sustained lysis of
404 phytoplankton has the potential to release DOC in a viral shunt near the mixolimnion-chemocline
405 transition. Such a DOC peak was observed slightly below this depth in Lake Cadagno. However,
406 given that VMR is a feature that emerges from a number of underlying virus-microbe, viral life
407 history traits, and environmental co-factors [52], the prediction of sustained phytoplankton viral
408 predation at the mixolimnion-chemocline transition requires empirical genomic confirmation.
409 Previous studies have identified genomic evidence for viral infection of the presumed
410 major carbon assimilators in the chemocline, *Thiodictyon syntrophicum,* and *Chromatium okenii*
411 [12]. Genomes of these organisms sequenced from Lake Cadagno contain CRISPR elements [41,42],
412 which derive from a type of acquired immunity against invading viral and plasmid DNA. This
413 suggests viruses may play a role in the modulation of carbon, and sulfur cycles, as has been
414 proposed in the study of a hydrothermal vent [53] and wetland [54] microbial communities, where
415 viruses have been found to carry genes central to methanogenesis (*mcrA*) and sulfur reduction
416 (*dsrA*, *dsrD*). Active viral lysis also provides a new possible mechanism to explain the previously
417 observed low abundance of *Chromatium okenii*, which was attributed to microbial predation [17].
418 Despite genomic evidence suggesting infection of these populations, VLP counts did not rise with
419 PLP counts in the chemocline. Yet, our observation of minimum VMR (Fig. 6M) and peak
420 microbial abundances in the Lake Cadagno chemocline support an emerging trend in stratified
421 meromictic lakes, as the same observation was made in meromictic Ace Lake (Vestfold Hills of
422 East Antarctica; [28]. Such coincident low VMR and high microbial abundance has been recognized
423 as a hallmark of the power-law relationship proposed to describe the VMR dynamics in aquatic
424 systems [52]. At the end, we suggest viruses as important part of Proterozoic ocean microbial
425 community and to resolve the rates and roles of infection on the evolution and function of microbes
426 that underlie Lake Cadagno biogeochemistry, especially in the chemocline, population-specific
427 studies of viral infection are needed to explain their detailed role from ancient ocean perspectives.
428 In the end, the organic matter facilitated by eukaryotes, bacteria and viruses in the
429 chemocline will eventually sink to sediments contributing to the organic matter burial (Fig. 6N).
430 Our empirical observations support the proposal that the chemocline (oxic-anoxic boundary) in
431 the ancient ocean [3] played a crucial role in transitioning from anoxygenic to oxygenic microbial
432 life, which dominated nutrient biogeochemical cycling in modern oceans [55,56].

Conclusion

This work summarizes how biogeochemical exchange within microbial guilds may be driving biomass accumulation in the permanently stratified Lake Cadagno. The observed trends emphasized the ecological importance of microbial guilds in stratified ancient oceans. In recent years, the pangenomes of the dominant chemocline anoxygenic phototrophs (*Thiodictyon syntrophicum*, *Chromatium okenii*) have been explored [41,47]. However, the genomes and metabolic potential of heterotrophic bacteria (e.g., *Lentimicrobium*) that recycle chemocline biomass in the presence of sulfur and ammonia are yet to be explored. Furthermore, eukaryotic phytoplankton in the deep chlorophyll max have been associated with the chemocline for at least two decades [18] and have survived hypoxia. Yet, insights into their cellular machinery that allows them to photosynthesize efficiently under limited light and oxygen is still missing. While primary producers (phytoplankton, and phototrophic sulfur bacteria) and heterotrophic bacteria are central to the realized function of the lake biogeochemistry and ecology, viruses may shuffle the repertoire of genes controlling both microbial guilds, hence modulating biogeochemical (carbon, nitrogen and sulfur) cycles of the lake. Future work will build from these observations to confirm such hypotheses.

Methodology

Water-sample collection and Physicochemical profiling

This study was conducted in Lake Cadagno (21 m deep), a high alpine meromictic lake situated at 1921 m above sea level in the Southern Alps of Switzerland [57]. Water sampling and characterization of physical (turbidity, temperature, oxygen, conductivity), biological (Chl *a*, phycocyanin) and chemical (H_2S, NH_4^+) parameters of the water column were performed as previously described [16]. Water was sampled on the 28 (Day 1) and 29 (Day 2) August 2017 using a double diaphragm teflon pump (Almatech PSG Germany Gmbh) connected to acid-washed low-density polyethylene (LDPE) line deployed from a platform that was anchored above the deepest part of the Lake Cadagno (46.55087° N, 8.71152° E). The oxic stratum of the lake (0-10 m) was sampled on 28 August (Day 1) and the chemocline and anoxic part strata (11-19 m) were sampled on 29 August 2017 (Day 2).

463 Vertical lake profiles were determined using an autonomous conductivity temperature
464 depth sensor (CTD; Ocean Seven 316 Plus CTD; IDRONAUT, S.R.L.). The CTD recorded
465 pressure (dbar), temperature (ºC), conductivity (mS/cm), and dissolved oxygen (mg/L) were
466 measured with a pressure-compensated polarographic sensor. The error in oxygen profiles for day
467 two was manually adjusted by referring to day 1 measurements which indicated approximately
468 zero oxygen within and below chemocline. CTD profiles from the whole water column (0-20 m,
469 Day 1 and 2) were used to identify the distribution of the mixolimnion, chemocline and
470 monimolimnion and guided water sampling strategy. The CTD was equipped with an LI-192
471 Underwater Quantum Sensor (Li-Cor Biosciences; NE, USA) that continuously recorded
472 photosynthetically active radiation (PAR-w/m^2;) and a TriLux multi-parameter algae sensor
473 (Chelsea Technologies Ltd; Surrey, UK) that measured in-vivo Chl *a* (Chl *a*, µg/L), an indicator
474 of phytoplankton (including eukaryotic autotrophs and cyanobacteria) biomass [58], and
475 phycocyanin (µg/L), a pigment characteristic of cyanobacteria [59].

476

477 **Chemical parameters**

478 *2.1 Dissolved compounds*

479 Samples for the analysis of dissolved compounds (DOC) were filtered through an Acropack filter
480 cartridge (PALL) with a 0.8 µm pre-filter and 0.2 µm final filter. Filters were collected in 30 mL
481 acid-washed and pyrolyzed pyrex tubes filled to the top and supplemented with 100 µL HCl 2M.
482 Tubes were stored in the dark at 4° C until processed (November 2017; University of the Geneva)
483 using a Shimadzu TOC-LCPH analysis system. Blanks consisting of Milli-Q water were made and
484 calibration was done using the standard from 0.2 to 5 ppm. Analyses of dissolved ammonium
485 (MNH_4^+) and hydrogen sulfide (H_2S) were done on-site at the Alpine Biology Centre (CBA; Piora,
486 Switzerland) with freshly collected water samples using a UV-visible spectrophotometer (DR
487 3800, HACH) [60].

488 *2.2 Particulate compounds*

489 Particulate organic carbon (POC), nitrogen (PON) and sulfur (POS) were collected by filtering
490 150 to 500 mL of lake water (volume necessary to begin to clog the filter) on pre-combusted 47
491 mm GF/F filters (5h at 550 °C, cat. #WH1825-047, Whatman, Wisconsin, USA), which were then

492 acidified (500 µL HCL 1 M, added twice at 1 h interval) and dried in an oven (65 °C) overnight in
493 acid-washed pyrex petri dishes. Samples were sealed using parafilm and aluminium foil until
494 analysis (November 2017, University of Geneva) using an Elemental Analyzer (2400 series II
495 CHNS/O Elemental Analysis, PerkinElmer). Procedural blanks using MilliQ water were
496 performed (24-25 November 2017) in duplicate to measure the background signal which was
497 subtracted to sample analysis. POC, PON, POS were expressed in mg/L (ppm).
498

499 **Biological parameters**

500 *3.1 Primary production*

501 Primary productivity was determined using incubation with $NaH_{14}CO_3$ (Perkin Elmer cat.
502 #NEC086H005MC; Waltham, MA, USA; 5 mCi, 1 mL in glass ampoule) that was freshly diluted
503 into 4 mL MilliQ water at pH 9.6 (adjusted using NaOH, Sigma) and added at a dose of 1 mCi/L
504 of lake water, as described [61]. Incubation experiment further explained in detail in supplementary
505 methodology.

506 *3.2 Maximum quantum yield*

507 The maximum quantum yield (F_v/F_m) informs the photosynthetic health and biological activity of
508 algae based on photo-physiological characteristics of the photosystem II variable Chl *a*
509 fluorescence. Maximum quantum yield was determined using a Fast Repetition Rate Fluorometer
510 (FRRF, FastOcean PTX coupled to a FastAct base unit; Chelsea Technologies). Water for
511 maximum quantum yield measurements was pre-concentrated 10-fold using a 47 mm filtration
512 unit (cat. #300-4000; Nalgene), a 0.2 µm 47 mm polycarbonate filter (cat. #GVWP04700,
513 Millipore; Darmstadt, Germany) and a 15 mL pipette to gently resuspend the cells as the sample
514 was passed through the filter using a hand pump (pressure below 15 mbar). This step was done to
515 ensure high enough method sensitivity and has been shown to alter neither Chl *a* nor cell integrity
516 of samples from Lake Geneva (Moisset et al., 2019). Please refer to supplementary methodology
517 for F_v/F_m calculations.

518 *3.3 Flow-cytometry*

519 A BD Accuri C6 cytometer (Becton Dickinson, San José CA, USA) was installed with two lasers

520 (blue: 488nm, red: 640 nm) and four fluorescence detectors (lasers 488 nm: FL1 = 533/30, FL2 =
521 585/40, FL3 = 670; laser 640 nm: FL4 = 675/25) was used to estimate total cell counts from fresh
522 unpreserved collected samples on-site in the Alpine Biology Centre. FL4 detectors were
523 specifically used to detect emission from phycobilin, a pigment proxy for cyanobacteria. Cells
524 were stained with SYBR green I (cat. #S7563, Molecular Probes; Eugene, OR) with a ratio of
525 1:10,000 (vol/vol), following incubation for 13 minutes at 37°C in the dark [11]. Histogram of event
526 counts versus green fluorescence (FL1 > 1,100) allowed quantification of total cells.

527 VLPs were counted using flow-cytometry after filtration of lake water through 55 µm mesh and
528 0.22 µm filters to remove large particles and cells. In triplicate, 1 ml sample from the filtrate was
529 fixed by adding 10 µL of glutaraldehyde (25% stock solution) in sample cryovials. The samples
530 were fixed for 15 minutes at room temperature and subsequently stored in liquid nitrogen for
531 shipping then stored at -80°C until processed in February 2018. Virus-like particle counts were
532 obtained using a FACSCalibur flow cytometer (Becton Dickinson Biosciences; Grenoble, France)
533 at Université Savoie Mont-Blanc. Samples were thawed at 37°C then diluted in a sterile buffer
534 solution of Tris-EDTA (0.1 mM Tris-HCL and 1 mM EDTA, pH 8) that had been autoclaved and
535 filtered through 0.02 µm. Samples were then stained for 10 minutes at 75°C using SYBR Green I
536 (Molecular Probes) at a 1:10,000 final concentration [62].

537 *3.3.2 Phenotypic alpha diversity of PLP (Prokaryotic-like-particles)*

538 Raw flow-cytometry files were used to estimate phenotypic traits (morphology and nucleic acid
539 content) using the Phenoflow package in R [37,63]. Briefly, this approach estimates kernel densities
540 on multiple bivariate single-cell parameter combinations (e.g., fluorescence and scatter intensity)
541 and concatenates these into a feature vector, which can be thought of as a phenotypic fingerprint
542 [37]. This fingerprint represents community structure in terms of the phenotypic attributes of the cells
543 that comprise the community—essentially, any feature that influences the way the laser interacts
544 with passing particles, such as morphology, size, and nucleic acid content, is captured in the
545 phenotypic fingerprint. Using this approach, bacterial phenotypic diversity metrics have been
546 shown to be highly correlated with community taxonomic diversity[37]. The phenotypic diversity
547 calculations are further explained in supplementary methodology.

548 *3.4 Secondary production*

549 Heterotrophic bacterial production also termed as secondary production was estimated by the
550 micro-centrifuge ^{3}H-Leucine bacterial production method [64], as described [65,66]. A working solution
551 of 5 µCi mL^{-1} leucine was made from a manufacturer stock solution of radioactive leucine, L-
552 [3,4,5-^{3}H(N)] (cat. #NET460A005MC, PerkinElmer, MA, USA). To reduce the potential for
553 autodegradation of the leucine radiolabel, this stock ^{3}H-Leucine material was stored in the dark at
554 2 to 4° C (never frozen) and used for the incorporation experiment within 5 days. Two replicates
555 and one trichloroacetic acid (TCA)-killed control (5% [vol/vol] final concentration; cat. 91228,
556 Sigma) were used for each depth. The details of secondary production are further described in
557 supplementary methodology .

558 *3.5 Statistics*

559 The magnitude and significance of linear relationships between physical and biological
560 parameters were determined with linear regression scatter plots in R-Studio (1.4.1106) using
561 ggplot2 (3.3.3)[67] and ggpubr (0.4.0) [68] packages which included correlation coefficients (R) with
562 p-values to the scatter plots [69]. R>0.70 was considered a strong correlation, and a p-value <0.05
563 was considered statistically significant.

564 **Illumina MiSeq 16S rRNA gene amplicon sequence analyses**

565 *4.1 16S rRNA gene amplicon sequencing*

566 The samples were collected from 3, 5, 7, 9, 11, 13, 15, 15.5, 17 and 19 m to capture Lake Cadagno's
567 mixolimnion (surface to 10 m), chemocline (11-14 m), and monimolimnion (below 16 m).
568 Collected water samples (20 L/depth) were 55 µm pre-filtered to remove large particles and
569 aggregates and then 0.22 µm filtered (cat. #GPWP14250 142 mm Express Plus Filter, Millipore;
570 Darmstadt, Germany) using a peristaltic pump. Filters were flash-frozen in liquid nitrogen and
571 stored at (-80°C) until extraction of DNA using the DNeasy Blood & Tissue Kit (cat. #69504
572 QIAGEN, Germantown, MD, USA) combined with QIAshredder (cat. #79654, QIAGEN, CA,
573 USA), as described [70]. The first and second elutions of DNA (50 µl each) were stored (4º C) until
574 sequencing. Dual indexed primers were used and the V4 region of the 16S rRNA gene amplicon
575 was targeted and amplified, as described [71]. Sequencing libraries were prepared using the Illumina

576 Nextera Flex kit (Illumina; CA, USA) and sequenced using the MiSeq platform (500 cycles,
577 Illumina) at the University of Michigan Microbiome Sequencing Core.
578 The 16S rRNA gene amplicon sequence reads were quality controlled and the contigs were
579 assembled, trimmed, aligned, and clustered into operational taxonomic units (OTUs) at 97%
580 identity threshold using mothur (Schloss et al., 2009). The OTUs were taxonomically classified
581 using SILVA (Quast et al. 2013) and TaxAss freshwater (Newton et al. 2011) 16S rRNA gene
582 databases. The code used for running the mothur analysis is available at the project GitHub
583 repository ([72]/). Raw sequences are available under project accession ID PRJNA717659 at NCBI.

584 *4.2 Genotypic alpha and beta diversity and Phylogenetic Tree*

585 Downstream analysis was carried out by the Phyloseq package in R-studio (v1.3.1093) to analyze
586 the alpha and beta genotypic diversity of bacterial communities. Taxa not observed in 20% of
587 samples at least 3 times were removed. The Alignment, Classification, and Tree (ACT) function
588 of SILVA was used to generate the phylogenetic tree [73]. Further steps of genotypic and phenotypic
589 diversity analysis are mentioned in supplementary methodology.

590 *4.3 Absolute Abundances (cells/ml)*

591 Absolute quantifications of taxa were determined as described [74]. The relative abundance of 16S
592 rRNA gene amplicons including bacteria and archaea of a given taxon (taxon read count/total read
593 count in sample) was multiplied by the PLP concentrations (cells/ml) for that sample, as
594 determined by flow cytometry. Thereon, archaeal abundance was deducted from the total
595 prokaryotic population to get an absolute abundance of the only bacterial population.
596
597 **Supplementary table**
598 SI Table
599
600 **Data and Code availability**
601 Data and code availability
602
603

Acknowledgements

The project was funded by Swiss National Science Foundation grant no. PP00P2-138955. We thank the University of Michigan microbiome core facility for sequencing Lake Cadagno 16S data. Many thanks to Dr. Sandro Peduzzi for providing housing during Lake Cadagno sampling, and for offering general comments on the manuscript. We also acknowledge BioRender for providing microbiology icons used in Fig. 6 schematic. Lastly, I, Jaspreet, express sincere gratitude to Swiss Confederation and Ernst and Lucy Schmidheiny Foundation for financially supporting me with a monthly salary which aided the development of this manuscript.

References

1. Canfield, D. E. A new model for Proterozoic ocean chemistry. *Nature* **396**, 450–453 (1998).
2. Reinhard, C. T., Raiswell, R., Scott, C., Anbar, A. D. & Lyons, T. W. A late Archean sulfidic sea stimulated by early oxidative weathering of the continents. *Science* **326**, 713–716 (2009).
3. Johnston, D. T., Wolfe-Simon, F., Pearson, A. & Knoll, A. H. Anoxygenic photosynthesis modulated Proterozoic oxygen and sustained Earth's middle age. *Proc. Natl. Acad. Sci. U. S. A.* **106**, 16925–16929 (2009).
4. Xiong, Y. *et al.* Phosphorus cycling in Lake Cadagno, Switzerland: A low sulfate euxinic ocean analogue. *Geochim. Cosmochim. Acta* **251**, 116–135 (2019).
5. Shen, Y., Buick, R. & Canfield, D. E. Isotopic evidence for microbial sulphate reduction in the early Archaean era. *Nature* **410**, 77–81 (2001).
6. Tonolla, M. *et al.* Lake Cadagno: Microbial Life in Crenogenic Meromixis. *Ecology of Meromictic Lakes* 155–186 (2017) doi:10.1007/978-3-319-49143-1_7.
7. *Ecology of meromictic lakes*. (Springer International Publishing, 2018).
8. Stewart, K. M., Walker, K. F. & Likens, G. E. Meromictic Lakes. in *Encyclopedia of Inland Waters* (ed. Likens, G. E.) 589–602 (Academic Press, 2009).

9. Wirth, S. B. *et al.* Combining sedimentological, trace metal (Mn, Mo) and molecular evidence for reconstructing past water-column redox conditions: The example of meromictic Lake Cadagno (Swiss Alps). *Geochim. Cosmochim. Acta* **120**, 220–238 (2013).
10. Philippi, M. *et al.* Purple sulfur bacteria fix N2 via molybdenum-nitrogenase in a low molybdenum Proterozoic ocean analogue. *Nat. Commun.* **12**, 4774 (2021).
11. Danza, F., Storelli, N., Roman, S., Lüdin, S. & Tonolla, M. Dynamic cellular complexity of anoxygenic phototrophic sulfur bacteria in the chemocline of meromictic Lake Cadagno. *PLoS One* **12**, e0189510 (2017).
12. Di Nezio, F. *et al.* Anoxygenic photo- and chemo-synthesis of phototrophic sulfur bacteria from an alpine meromictic lake. *FEMS Microbiol. Ecol.* **97**, (2021).
13. Halm, H. *et al.* Co-occurrence of denitrification and nitrogen fixation in a meromictic lake, Lake Cadagno (Switzerland). *Environ. Microbiol.* **11**, 1945–1958 (2009).
14. Storelli, N. *et al.* CO_2 assimilation in the chemocline of Lake Cadagno is dominated by a few types of phototrophic purple sulfur bacteria. *FEMS Microbiol. Ecol.* **84**, 421–432 (2013).
15. Posth, N. R. *et al.* Carbon isotope fractionation by anoxygenic phototrophic bacteria in euxinic Lake Cadagno. *Geobiology* **15**, 798–816 (2017).
16. Ellwood, M. J. *et al.* Iron isotope transformations in the meromictic Lake Cadagno. *Geochim. Cosmochim. Acta* **255**, 205–221 (2019).
17. Musat, N. *et al.* A single-cell view on the ecophysiology of anaerobic phototrophic bacteria. *Proc. Natl. Acad. Sci. U. S. A.* **105**, 17861–17866 (2008).
18. Camacho, A. *et al.* Microbial microstratification, inorganic carbon photoassimilation and dark carbon fixation at the chemocline of the meromictic Lake Cadagno (Switzerland) and

its relevance to the food web. *Aquat. Sci.* **63**, 91–106 (2001).

19. Falkowski, P. G. *et al.* The evolution of modern eukaryotic phytoplankton. *Science* **305**, 354–360 (2004).
20. Hurley, S. J., Wing, B. A., Jasper, C. E., Hill, N. C. & Cameron, J. C. Carbon isotope evidence for the global physiology of Proterozoic cyanobacteria. *Sci Adv* **7**, (2021).
21. Hamilton, T. L., Bryant, D. A. & Macalady, J. L. The role of biology in planetary evolution: cyanobacterial primary production in low-oxygen Proterozoic oceans. *Environ. Microbiol.* **18**, 325–340 (2016).
22. Suttle, C. A. Marine viruses--major players in the global ecosystem. *Nat. Rev. Microbiol.* **5**, 801–812 (2007).
23. Winget, D. M. *et al.* Repeating patterns of virioplankton production within an estuarine ecosystem. *Proc. Natl. Acad. Sci. U. S. A.* **108**, 11506–11511 (2011).
24. Breitbart, M., Bonnain, C., Malki, K. & Sawaya, N. A. Phage puppet masters of the marine microbial realm. *Nat Microbiol* **3**, 754–766 (2018).
25. Zimmerman, A. E. *et al.* Metabolic and biogeochemical consequences of viral infection in aquatic ecosystems. *Nat. Rev. Microbiol.* **18**, 21–34 (2020).
26. Weinbauer, M. G. *et al.* Viral ecology of organic and inorganic particles in aquatic systems: avenues for further research. *Aquat. Microb. Ecol.* **57**, 321–341 (2009).
27. Zhao, Z. *et al.* Microbial transformation of virus-induced dissolved organic matter from picocyanobacteria: coupling of bacterial diversity and DOM chemodiversity. *ISME J.* **13**, 2551–2565 (2019).
28. Lauro, F. M. *et al.* An integrative study of a meromictic lake ecosystem in Antarctica. *ISME J.* **5**, 879–895 (2011).

676 29. Sime-Ngando, T. *et al.* Lake Pavin: A Pioneer Site for Ecological Studies of Freshwater
677 Viruses. in *Lake Pavin: History, geology, biogeochemistry, and sedimentology of a deep*
678 *meromictic maar lake* (eds. Sime-Ngando, T., Boivin, P., Chapron, E., Jezequel, D. &
679 Meybeck, M.) 229–244 (Springer International Publishing, 2016).
680 30. Wu, Y.-T. *et al.* Comprehensive Insights Into Composition, Metabolic Potentials, and
681 Interactions Among Archaeal, Bacterial, and Viral Assemblages in Meromictic Lake Shunet
682 in Siberia. *Front. Microbiol.* **9**, 1763 (2018).
683 31. Christie-Oleza, J. A., Sousoni, D., Lloyd, M., Armengaud, J. & Scanlan, D. J. Nutrient
684 recycling facilitates long-term stability of marine microbial phototroph-heterotroph
685 interactions. *Nat Microbiol* **2**, 17100 (2017).
686 32. Coutinho, F. H. *et al.* Marine viruses discovered via metagenomics shed light on viral
687 strategies throughout the oceans. *Nature Communications* vol. 8 (2017).
688 33. Vaquer-Sunyer, R. & Duarte, C. M. Thresholds of hypoxia for marine biodiversity. *Proc.*
689 *Natl. Acad. Sci. U. S. A.* **105**, 15452–15457 (2008).
690 34. Tonolla, M., Demarta, A., Peduzzi, S., Hahn, D. & Peduzzi, R. In situ analysis of sulfate-
691 reducing bacteria related to Desulfocapsa thiozymogenes in the chemocline of meromictic
692 Lake Cadagno (Switzerland). *Appl. Environ. Microbiol.* **66**, 820–824 (2000).
693 35. Peduzzi, S., Tonolla, M. & Hahn, D. Isolation and characterization of aggregate-forming
694 sulfate-reducing and purple sulfur bacteria from the chemocline of meromictic Lake
695 Cadagno, Switzerland. *FEMS Microbiol. Ecol.* **45**, 29–37 (2003).
696 36. Pruesse, E. *et al.* SILVA: a comprehensive online resource for quality checked and aligned
697 ribosomal RNA sequence data compatible with ARB. *Nucleic Acids Res.* **35**, 7188–7196
698 (2007).

37. Props, R., Monsieurs, P., Mysara, M., Clement, L. & Boon, N. Measuring the biodiversity of microbial communities by flow cytometry. *Methods Ecol. Evol.* **7**, 1376–1385 (2016).

38. Cabrera, S., López, M. & Tartarotti, B. Phytoplankton and zooplankton response to ultraviolet radiation in a high-altitude Andean lake: short- versus long-term effects. *J. Plankton Res.* **19**, 1565–1582 (1997).

39. Danza, F. *et al.* Bacterial diversity in the water column of meromictic Lake Cadagno and evidence for seasonal dynamics. *PLoS One* **13**, e0209743 (2018).

40. Luedin, S. M. *et al.* Mixotrophic Growth Under Micro-Oxic Conditions in the Purple Sulfur Bacterium 'Thiodictyon syntrophicum'. *Front. Microbiol.* **10**, 384 (2019).

41. Luedin, S. *et al.* Draft Genome Sequence of Chromatium okenii Isolated from the Stratified Alpine Lake Cadagno. *Sci. Rep.* **9**, 1936 (2019).

42. Luedin, S. M. *et al.* Complete genome sequence of 'Thiodictyon syntrophicum' sp. nov. strain Cad16T, a photolithoautotrophic purple sulfur bacterium isolated from the alpine meromictic Lake Cadagno. *Stand. Genomic Sci.* **13**, 14 (2018).

43. Brocks, J. J. *et al.* Biomarker evidence for green and purple sulphur bacteria in a stratified Palaeoproterozoic sea. *Nature* **437**, 866–870 (2005).

44. Berg, J. S. *et al.* Dark aerobic sulfide oxidation by anoxygenic phototrophs in anoxic waters. *Environ. Microbiol.* **21**, 1611–1626 (2019).

45. Milucka, J. *et al.* Methane oxidation coupled to oxygenic photosynthesis in anoxic waters. *ISME J.* **9**, 1991–2002 (2015).

46. Berg, J. S. *et al.* Intensive cryptic microbial iron cycling in the low iron water column of the meromictic Lake Cadagno. *Environ. Microbiol.* **18**, 5288–5302 (2016).

47. Peduzzi, S. *et al.* Candidatus 'Thiodictyon syntrophicum', sp. nov., a new purple sulfur

722 bacterium isolated from the chemocline of Lake Cadagno forming aggregates and specific
723 associations with Desulfocapsa sp. *Systematic and Applied Microbiology* vol. 35 139–144
724 (2012).
725 48. Sun, L. *et al.* Lentimicrobium saccharophilum gen. nov., sp. nov., a strictly anaerobic
726 bacterium representing a new family in the phylum Bacteroidetes, and proposal of
727 Lentimicrobiaceae fam. nov. *Int. J. Syst. Evol. Microbiol.* **66**, 2635–2642 (2016).
728 49. Voorhies, A. A. *et al.* Ecological and genetic interactions between cyanobacteria and
729 viruses in a low-oxygen mat community inferred through metagenomics and
730 metatranscriptomics. *Environ. Microbiol.* **18**, 358–371 (2016).
731 50. Howard-Varona, C. *et al.* Phage-specific metabolic reprogramming of virocells. *The ISME*
732 *Journal* vol. 14 881–895 (2020).
733 51. Yau, S. *et al.* Virus-host coexistence in phytoplankton through the genomic lens. *Sci Adv* **6**,
734 eaay2587 (2020).
735 52. Wigington, C. H. *et al.* Re-examination of the relationship between marine virus and
736 microbial cell abundances. *Nat Microbiol* **1**, 15024 (2016).
737 53. Anantharaman, K. *et al.* Sulfur oxidation genes in diverse deep-sea viruses. *Science* **344**,
738 757–760 (2014).
739 54. Dalcin Martins, P. *et al.* Viral and metabolic controls on high rates of microbial sulfur and
740 carbon cycling in wetland ecosystems. *Microbiome* **6**, 138 (2018).
741 55. Azam, F. & Malfatti, F. Microbial structuring of marine ecosystems. *Nat. Rev. Microbiol.* **5**,
742 782–791 (2007).
743 56. Zhang, C. *et al.* Evolving paradigms in biological carbon cycling in the ocean. *Natl Sci Rev*
744 **5**, 481–499 (2018).

57. Del Don, C., Hanselmann, K. W., Peduzzi, R. & Bachofen, R. The meromictic alpine Lake Cadagno: Orographical and biogeochemical description. *Aquat. Sci.* **63**, 70–90 (2001).

58. Martinez, E. *et al.* Reconstructing global chlorophyll-a variations using a non-linear statistical approach. *Front. Mar. Sci.* **7**, (2020).

59. Ogashawara, I. Determination of Phycocyanin from Space—A Bibliometric Analysis. *Remote Sensing* **12**, 567 (2020).

60. Bridgewater, L., American Public Health Association, American Water Works Association & Water Environment Federation. *Standard Methods for the Examination of Water and Wastewater*. (American Public Health Association, 2012).

61. Hassler, C. S. *et al.* Primary productivity induced by iron and nitrogen in the Tasman Sea: an overview of the PINTS expedition. *Mar. Freshwater Res.* **65**, 517–537 (2014).

62. Jacquet, S., Dorigo, U. & Personnic, S. A few tests prior to flow cytometry and epifluorescence analyses of freshwater bacterio-and virioplankton communities. *FLOW Cytom* **1**, 1–30 (2013).

63. *Phenoflow_package*. (Github).

64. Smith, D. C. & Azam, F. A simple, economical method for measuring bacterial protein synthesis rates in seawater using 3H-leucine. *Mar. Microb. Food Webs* **6**, 107–114 (1992).

65. Kirchman, D. L., Keel, R. G., Simon, M. & Welschmeyer, N. A. Biomass and production of heterotrophic bacterioplankton in the oceanic subarctic Pacific. *Deep Sea Res. Part I* **40**, 967–988 (1993).

66. Fourquez, M. *et al.* Microbial Competition in the Subpolar Southern Ocean: An Fe–C Co-limitation Experiment. (2020) doi:10.3389/fmars.2019.00776.

67. Wickham, H. Ggplot2. *Wiley Interdiscip. Rev. Comput. Stat.* **3**, 180–185 (2011).

768 68. Kassambara, A. ggpubr:'ggplot2' based publication ready plots (Version 0.1. 7). *Obtido*
769 *desde https://CRAN. R-project. org/package= ggpubr* (2018).
770 69. Wei, T. & Simko, V. R package 'corrplot': Visualization of a Correlation Matrix (Version
771 0.84). (2017).
772 70. Duhaime, M. & Cable, R. DNA Extraction from Filters using QIAgen DNeasy and
773 QIAshredder v1 (protocols.io.jx5cpq6). *protocols.io* (2017)
774 doi:10.17504/protocols.io.jx5cpq6.
775 71. Kozich, J. J., Westcott, S. L., Baxter, N. T., Highlander, S. K. & Schloss, P. D.
776 Development of a dual-index sequencing strategy and curation pipeline for analyzing
777 amplicon sequence data on the MiSeq Illumina sequencing platform. *Appl. Environ.*
778 *Microbiol.* **79**, 5112–5120 (2013).
779 72. *Lake_Cadagno_microbial_loop_Saini_et_al_2021*. (Github).
780 73. Pruesse, E., Peplies, J. & Glöckner, F. O. SINA: accurate high-throughput multiple
781 sequence alignment of ribosomal RNA genes. *Bioinformatics* **28**, 1823–1829 (2012).
782 74. Props, R. *et al.* Absolute quantification of microbial taxon abundances. *ISME J.* **11**, 584–
783 587 (2017).

Supplementary figures

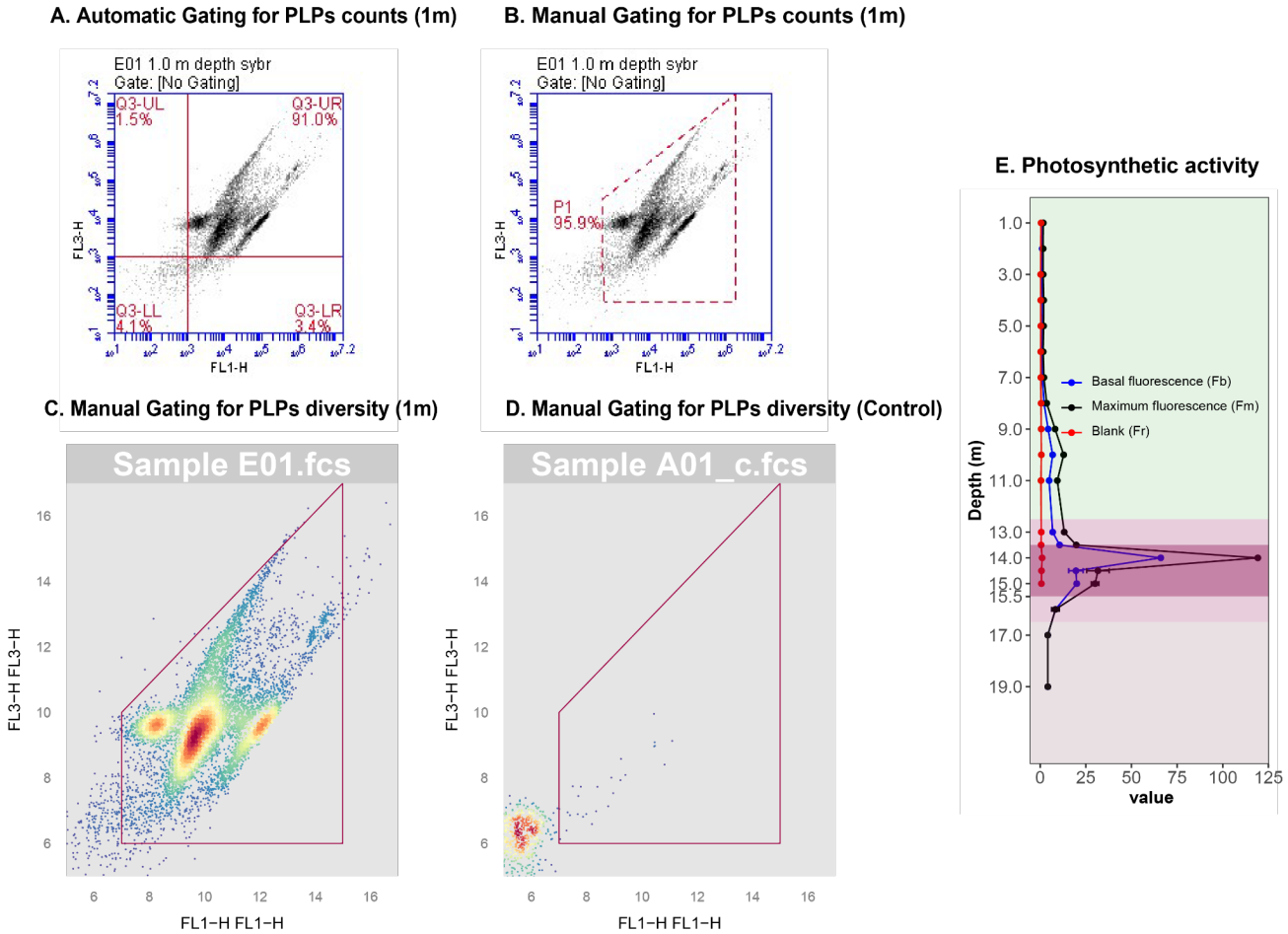

Fig. S1: Raw flow-cytometry files visualized with; BD6 flow-cytometer interface (A-B) and R-studio Phenoflow package (A-D). Red outline represents the gating strategy for cell counting and phenotypic diversity analysis. FCM events representing prokaryotic-like particles in a Lake Cadagno (1 m depth) targeted using (A) Four-area layout vs (B,C) Manual coordinated based gating. (D) FCM events represent prokaryotic-like particles in a 0.2 µm filtered, cell-free MilliQ water (control). (E) Experiment to monitor the health of photosynthetic cells. Basal fluorescence (F_b) and maximum fluorescence (F_m) were obtained to calculate Fv/Fm values.

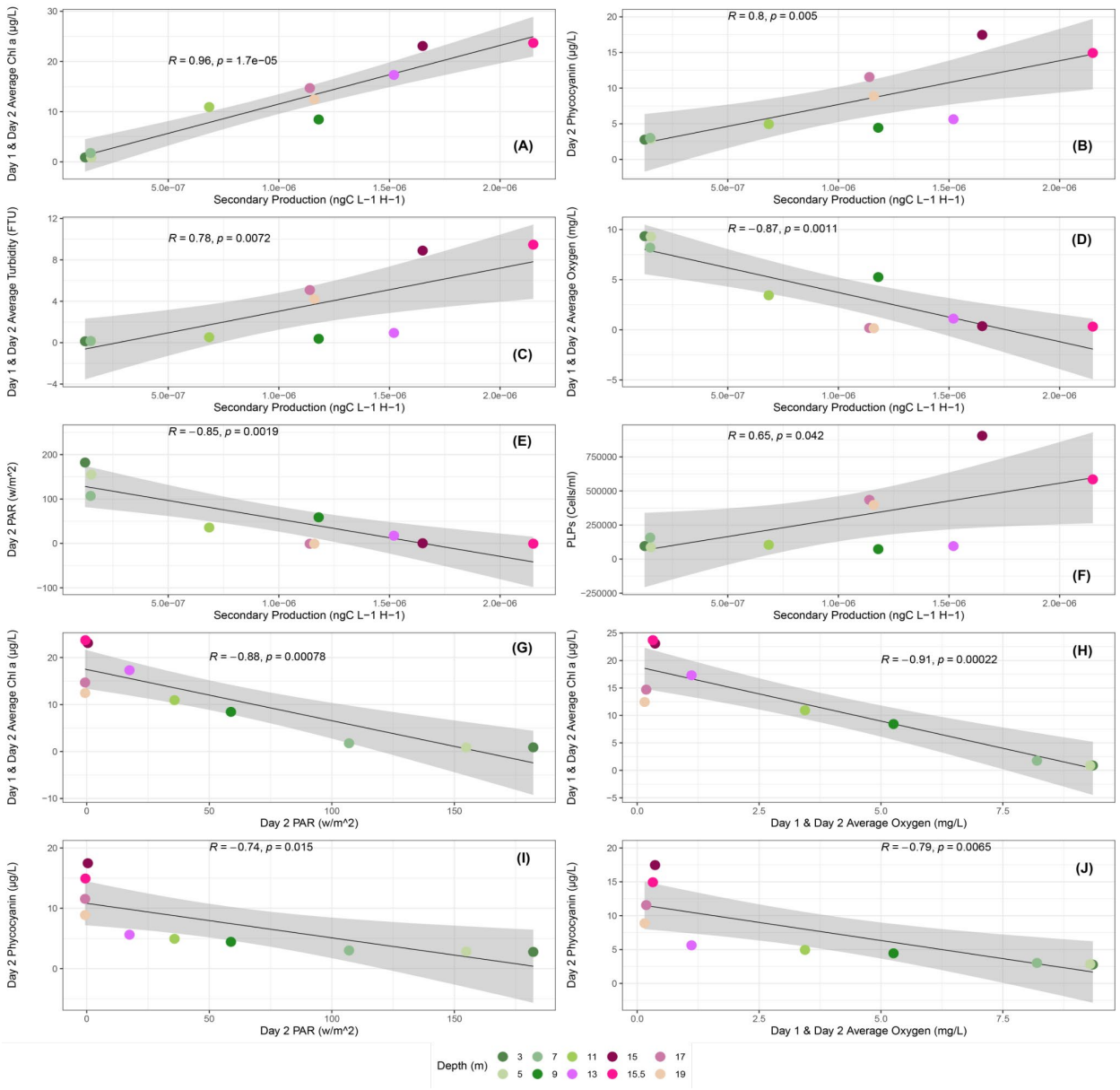
(A)
R = 0.96, p = 1.7e−05
Day 1 & Day 2 Average Chl a (µg/L)
Secondary Production (ngC L−1 H−1)
(B)
R = 0.8, p = 0.005
Day 2 Phycocyanin (µg/L)
Secondary Production (ngC L−1 H−1)
(C)
R = 0.78, p = 0.0072
Day 1 & Day 2 Average Turbidity (FTU)
Secondary Production (ngC L−1 H−1)
(D)
R = −0.87, p = 0.0011
Day 1 & Day 2 Average Oxygen (mg/L)
Secondary Production (ngC L−1 H−1)
(E)
R = −0.85, p = 0.0019
Day 2 PAR (w/m^2)
Secondary Production (ngC L−1 H−1)
(F)
R = 0.65, p = 0.042
PLPs (Cells/ml)
Secondary Production (ngC L−1 H−1)
(G)
R = −0.88, p = 0.00078
Day 1 & Day 2 Average Chl a (µg/L)
Day 2 PAR (w/m^2)
(H)
R = −0.91, p = 0.00022
Day 1 & Day 2 Average Chl a (µg/L)
Day 1 & Day 2 Average Oxygen (mg/L)
(I)
R = −0.74, p = 0.015
Day 2 Phycocyanin (µg/L)
Day 2 PAR (w/m^2)
(J)
R = −0.79, p = 0.0065
Day 2 Phycocyanin (µg/L)
Day 1 & Day 2 Average Oxygen (mg/L)
Depth (m)
3 5 7 9 11 13 15 15.5 17 19

796

Fig. S2 R-coefficient and p-values were obtained using linear regression performed between secondary production, photosynthetic pigments, Prokaryotic-like-particles (PLPs), and physicochemical parameters including turbidity, oxygen and light. Lake depth in meters (m) is indicated by colors. (A) Secondary production vs Chl a (B) Secondary production vs Phycocyanin (C) Secondary production vs Turbidity (D) Secondary production vs Oxygen (E) Secondary production vs light (F) Secondary production vs PLPs (G-J) Chl a and Phycocyanin vs oxygen and light.

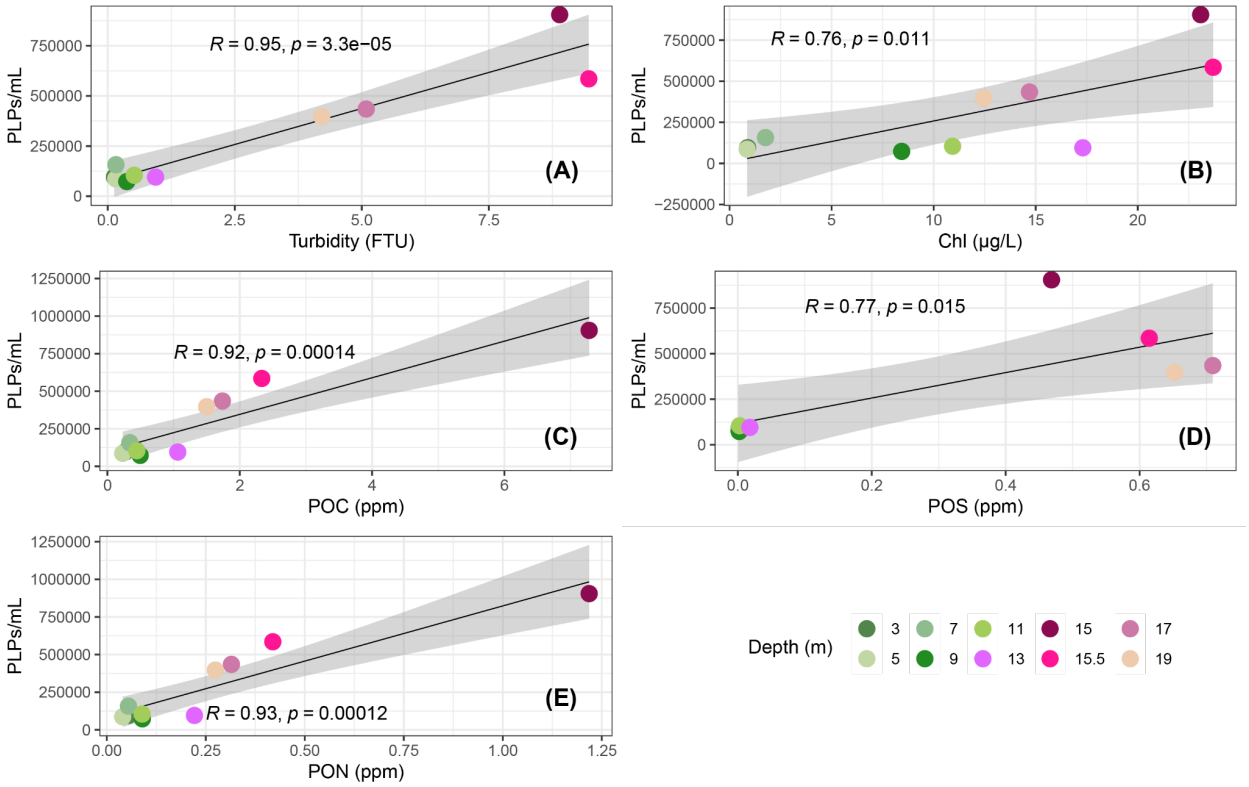

Fig. S3 R-coefficient and p-values were obtained using linear regression performed between Prokaryotic-like-particles (PLPs) and biomass indicating factors. Lake depth in meters (m) is indicated by colors. (A) PLPs vs Turbidity (B) PLPs vs Chl a (C) PLPs vs particulate organic carbon (POC). (D) PLPs vs particulate organic sulfur (POS). (E) PLPs vs particulate organic nitrogen (PON).

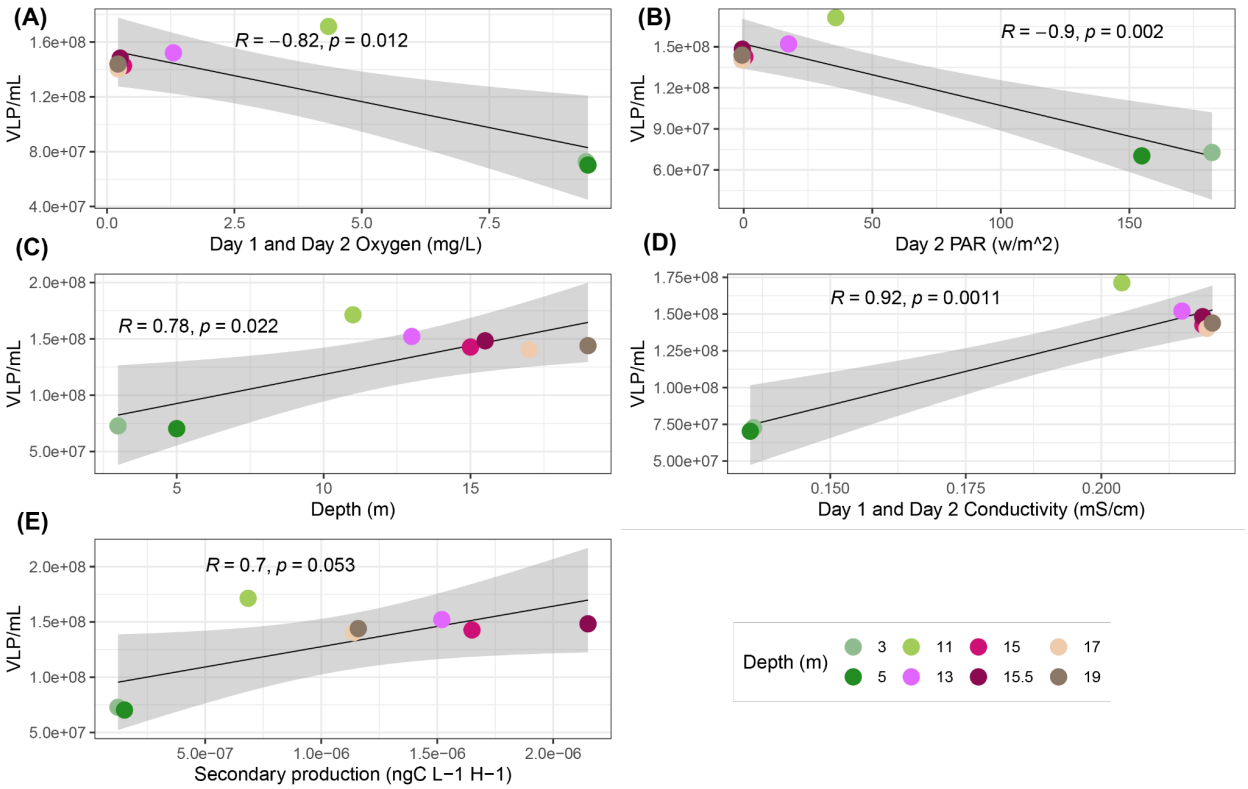

Fig. S4 R-coefficient and p-values were obtained using linear regression performed between Virus-like-particles (PLPs) and physicochemical parameters. Lake depth in meters (m) is indicated by colors. (A) VLPs vs Oxygen (B) VLPs vs Light (C) VLPs vs depth. (D) VLPs vs conductivity. (E) VLPs vs secondary production.

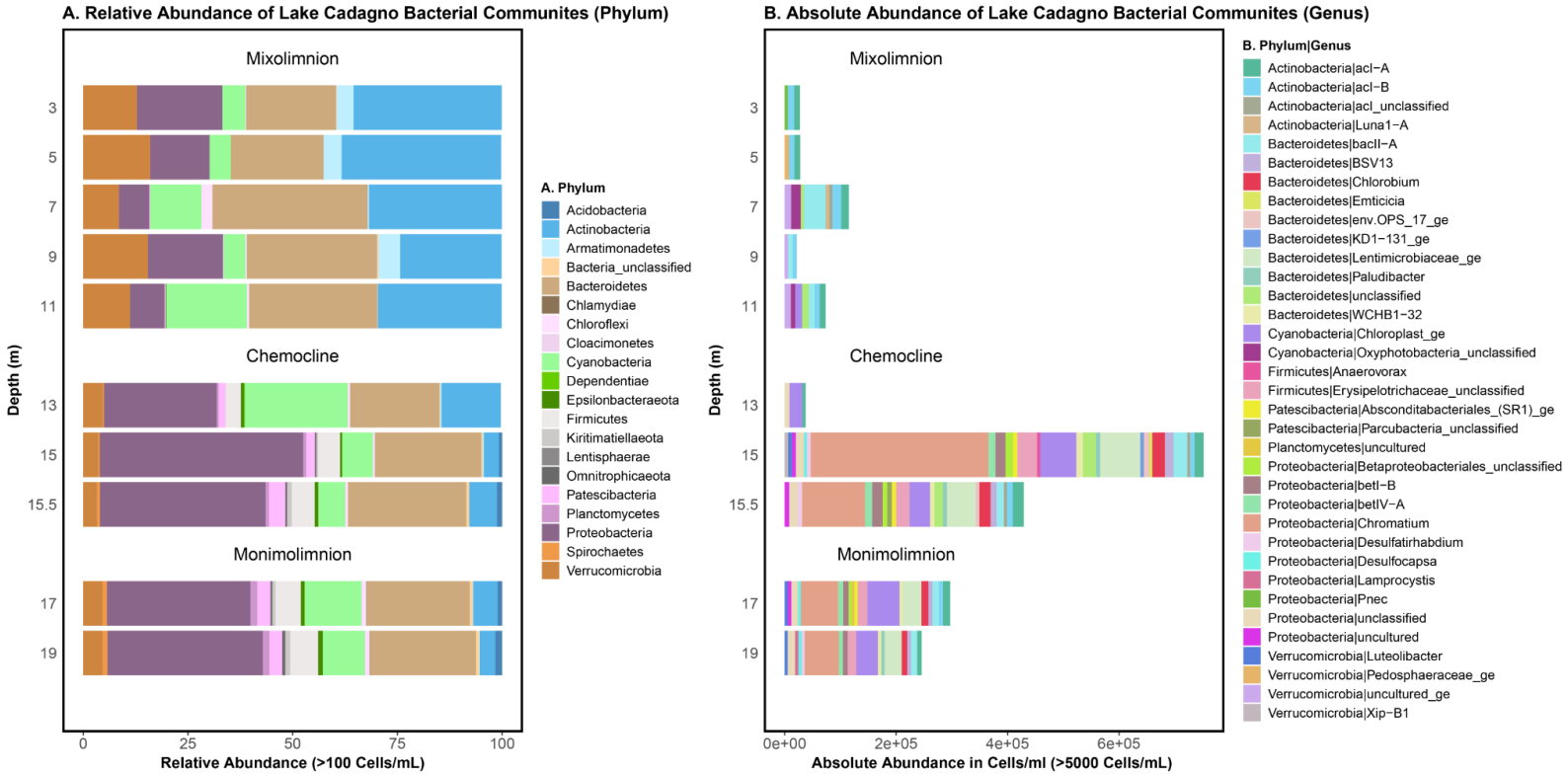

Fig. S5 Relative and absolute abundance of microbial cells based on 16S reads and flow-cytometry cells counts within the vertical water column of Lake Cadagno. (A) 16S relative abundance of bacterial communities at phylum.(B) Absolute abundance of bacterial communities based on 16S and flow-cytometry cell counts at genus level.

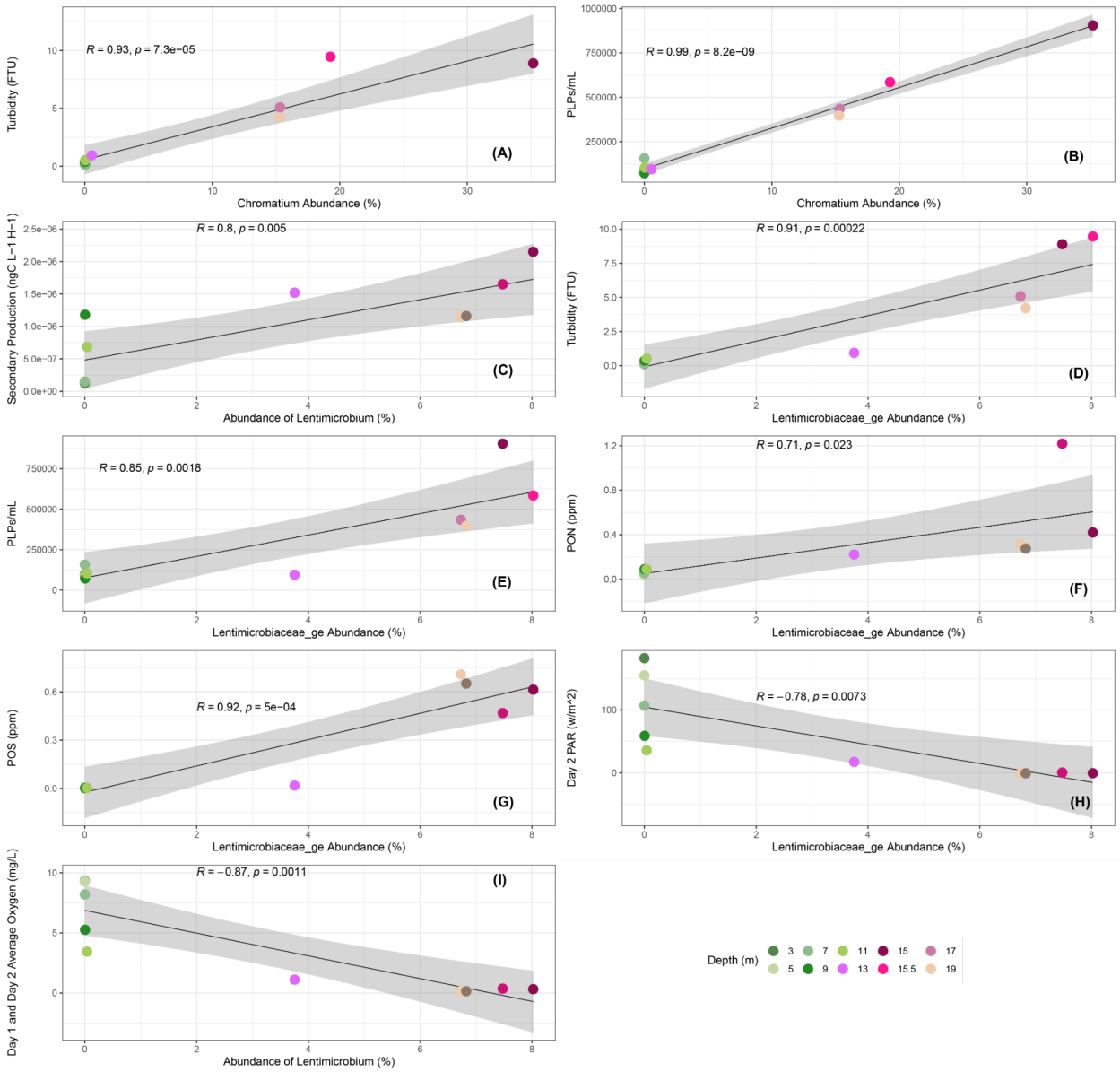

Fig. S6 R-coefficient and p-values were obtained using linear regression performed between microbial abundance and physicochemical parameters. Lake depth in meters (m) is indicated by colors. (A-B) Chromatium vs PLPs and turbidity. (C-I) Lentimicrobium vs secondary productivity, turbidity, PLPs, PON, POS, light and oxygen.

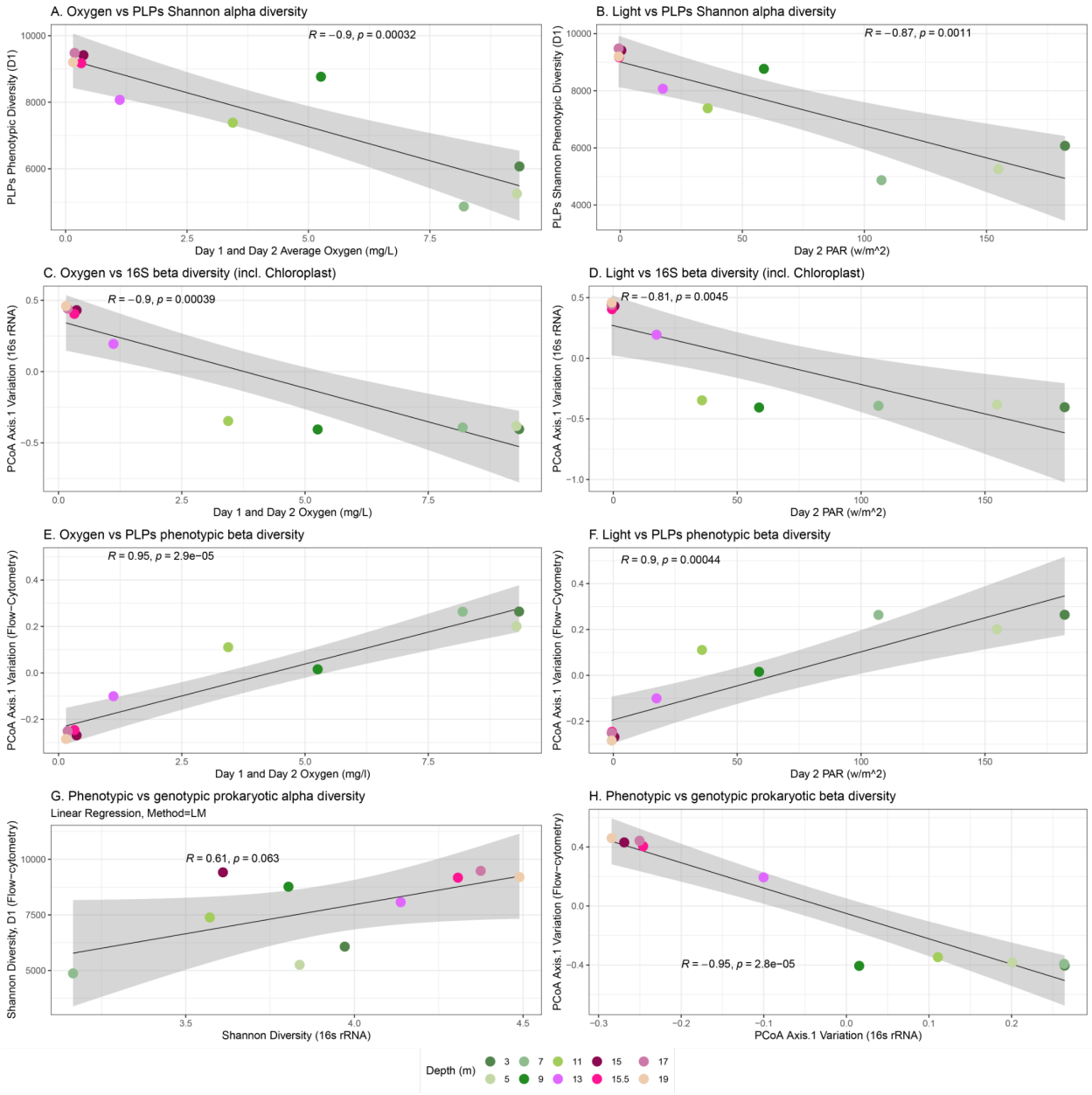
A. Oxygen vs PLPs Shannon alpha diversity
R = −0.9, p = 0.00032
PLPs Phenotypic Diversity (D1)
Day 1 and Day 2 Average Oxygen (mg/L)
B. Light vs PLPs Shannon alpha diversity
R = −0.87, p = 0.0011
PLPs Shannon Phenotypic Diversity (D1)
Day 2 PAR (w/m^2)
C. Oxygen vs 16S beta diversity (incl. Chloroplast)
R = −0.9, p = 0.00039
PCoA Axis.1 Variation (16s rRNA)
Day 1 and Day 2 Oxygen (mg/L)
D. Light vs 16S beta diversity (incl. Chloroplast)
R = −0.81, p = 0.0045
PCoA Axis.1 Variation (16s rRNA)
Day 2 PAR (w/m^2)
E. Oxygen vs PLPs phenotypic beta diversity
R = 0.95, p = 2.9e−05
PCoA Axis.1 Variation (Flow−Cytometry)
Day 1 and Day 2 Oxygen (mg/l)
F. Light vs PLPs phenotypic beta diversity
R = 0.9, p = 0.00044
PCoA Axis.1 Variation (Flow−Cytometry)
Day 2 PAR (w/m^2)
G. Phenotypic vs genotypic prokaryotic alpha diversity
Linear Regression, Method=LM
R = 0.61, p = 0.063
Shannon Diversity, D1 (Flow−cytometry)
Shannon Diversity (16s rRNA)
H. Phenotypic vs genotypic prokaryotic beta diversity
R = −0.95, p = 2.8e−05
PCoA Axis.1 Variation (Flow−cytometry)
PCoA Axis.1 Variation (16s rRNA)
Depth (m)
3 5 7 9 11 13 15 15.5 17 19

850 Fig. S7 R-coefficient and p-values were obtained using linear regression performed between
851 microbial alpha and beta diversity and physicochemical parameters. Lake depth in meters (m) is
852 indicated by colors. (A-B) PLPs Shannon alpha diversity vs oxygen and light. (C-D) 16S beta
853 diversity vs oxygen and light. (E,F) PLP phenotypic beta diversity vs oxygen and light. (G-H)
854 Phenotypic vs genotypic prokaryotic alpha and beta diversity.
855
856 **Supplementary methodology**

857 *3.1 Primary productivity*

858 Incubation was carried out along an incubation chain deployed at 6 depths for 23 h on 28-29
859 August 2017. Each depth consisted of a metallic ring fixed to a rope at the desired depth (3, 5, 7,
860 9, 11 and 13 m). The ring was surrounded by 6 arms on a horizontal plane, each of which ended
861 with a bottle holder. 75 mL acid-washed glass bottles were filled to the top with lake water (ca.
862 100 mL) at the corresponding depth and spiked with ^{14}C prior to being deployed on each level of
863 the incubation chain. At each depth, three transparent bottles were incubated for activity
864 measurements at *in situ* natural light intensities and three amber bottles were incubated for dark
865 community respiration measurements. At the end of the incubation, each bottle was filtered onto
866 47 mm GF/F filters (cat. #WH1825-047, Whatman, Wisconsin, USA) that were then each stored
867 in a plastic petri dish. Petri dishes were placed in a sealed box containing calcium hydroxide
868 (slaked lime) powder. After adding HCL (1M, 500 µL) onto filters, inorganic carbon was allowed
869 to degas overnight in a sealed box. Filters were then collected into 20 ml scintillation vials,
870 supplemented with 10 mL of Ultima Gold AB cocktail, and shaken manually. Slaked lime, Decon
871 solution and pipet tips were collected as radioactive waste for appropriate disposal at the
872 University of Geneva, while all other labware was decontaminated by using warm (40 to 50° C)
873 5% solution of Decon 90 (cat no. #10335650, East Sussex, England). Primary productivity was
874 expressed in µmol of carbon net fixation per h either per L of lake water or per Chl *a,* considering
875 a dissolved inorganic carbon concentration of 1.8 mM C [20].
876

877 *3.2 Maximum quantum yield*

878 The FRRF was used in single turnover mode to record, in a 45 min dark-adapted natural sample,
879 the basal (F_b) and the maximal (F_m) fluorescence following exposure to intense light. The sample

880 was then gently filtered on a 0.2 µm 47 mm syringe filter (cat. #GVWP04700, Millipore;
881 Darmstadt, Germany) to record the residual fluorescence (F_r). For each sample, the F_b-F_r
882 represented the initial dark-adapted fluorescence F_0 associated with intact cells. The F_v/F_m was
883 then calculated using the ratio: $(F_m - F_0)/F_m$.

884 *3.3.2 Phenotypic alpha diversity of PLP (Prokaryotic-like-particles)*

885 To calculate phenotypic alpha diversity, phenoflow calculates Hill number diversity indices (D_q)
886 from order 0-2, where 0 represents the richness and q>1 represents richness and evenness also
887 referred to as D0 (richness), D1 (Shannon), and D2 (inverse Simpson) [46]. Phenotypic beta diversity
888 was estimated using PCoA of phenotypic fingerprints.

889 Fluorescence detectors (lasers 488 nm: FL1-H = 533/30, FL3-H = 670) were used to target PLP
890 diversity. Polygon gating was applied to filter out the noise observed in control samples (Fig. S1).
891 Clockwise, the polygon gate coordinates (x,y) were: (7, 6), (15, 6), (15, 17), and (7,10). Kernel
892 density estimates were calculated by applying binning grid (128 x 128) to FSC-H (Forward scatter
893 height), SSC-H (Side scatter height), FL1-H and FL3-H. The obtained kernel densities values were
894 assigned into one-dimensional vectors, termed *phenotypic fingerprints*.
895

896 *3.4 Secondary production*

897 Briefly, 1.5-mL of lake water samples were incubated with a mixture of radioactive and
898 nonradioactive leucine at final concentrations of 20 nM. Using the [^{3}H]-Leucine working solution,
899 enough "hot" leucine was added to each tube to create a sufficient signal (50% or 85% of hot
900 leucine were used in the mixture for samples collected above and below 13m depths, respectively).
901 Incubations were conducted in a dark incubator at the respective *in situ* temperatures
902 (corresponding to the depths) for 2 h. Saturation of leucine incorporation over this period was
903 tested with 20, 30 and 40 nM of total leucine. At the end of the incubation, 200 µL of 50% TCA
904 is added to all but the control tubes to terminate leucine incorporation. To facilitate the
905 precipitation of proteins, bovine serum albumin (BSA; Sigma, 100 mgL^{-1} final concentration) was
906 added, then samples were centrifuged at 16,000 g for 10 min [50]. The supernatant was discarded
907 and the resultant precipitated proteins were washed with 1.5 mL of 5% TCA by vigorous vortexing
908 and again centrifuged (16,000 g for 10 min). The supernatant was discarded. Subsequently, 1.5
909 mL of UltimaGoldTM uLLt (Part number: 6013681, PerkinElmer, MA, USA) was added to each

910 vial, mixed, and allowed to sit for >24 h before the radioactivity was determined by liquid
911 scintillation using a Beckman LS6500 liquid scintillation counter. To calculate biomass
912 production, the following conversion factors were applied: molecular weight of leucine of 131.2
913 g/mol, a fraction of leucine per protein of 0.073), the ratio of cellular carbon to the protein of 0.86,
914 and 2.22×10^6 DPM/µCi to convert disintegrations per minute (DPMs; the measure of radioactivity)
915 to µCi. A factor of 1.55 kg C mol leucine^{-1} was used to convert the incorporation of leucine to
916 carbon equivalents, assuming no isotope dilution [51].

917 *4.2 Genotypic alpha and beta diversity and Phylogenetic Tree*

918 Representative sequences of chloroplast OTUs were aligned to SILVA sequences (SINA 1.2.11)
919 Two neighbours per query sequence (95% minimum sequence identity) were added to the tree with
920 the chloroplast OTU sequences. Advance variability profile was selected as 'auto' and sequences
921 below 90% identity were rejected. The phylogenetic tree of the OTUs was bootstrapped with
922 RAxML [59] with 20 maximum likelihood (ML) and 100 bootstrapped searches. Annotation was
923 performed in R-studio (1.4.1106) with package ggtree (2.2.4) and Adobe Illustrator (25.2.1).
924